ONLINE MONITORING OF OUTDOOR NON-CERAMIC INSULATORS

A THESIS IN ELECTRICAL ENGINEERING

Presented to the faculty of the American University of Sharjah
College of Engineering
in partial fulfillment of
the requirements for the degree

MASTER OF SCIENCE

By

IBRAHIM YEHIA SHURRAB

B.S. 2007

Sharjah, UAE

June 2011

We approve the thesis of *Ibrahim Yehia Shurrab* Date of signature

_____ _____

Dr. Ayman El-Hag
Assistant Professor
Thesis Advisor

_____ _____

Dr. Khaled Assaleh
Associate Professor
Thesis Advisor

_____ _____

_____ _____

_____ _____

_____ _____

ONLINE MONITORING OF OUTDOOR NON-CERAMIC INSULATORS

Ibrahim Yehia Shurrab, Candidate for the Master of Science Degree

American University of Sharjah, 2011

ABSTRACT

Transmitting power using overhead lines is heavily used by power utilities due to their lower cost compared with underground cables. However, overhead lines have shown great influence on power system due to frequent power interruption caused insulator failure. Power interruption is a critical issue facing utility companies in terms of huge financial loss by both utility, unpaid interruption hours, and customers, especially industrial customers. Insulator failure is the core reason of power interruption; therefore, failure of outdoor insulator should receive great attention and analysis.

Overhead line insulators are mainly of two types: ceramic and composite insulators. Composite insulators are now replacing ceramic insulators especially in extra high voltage applications because of their low weight, vandalism resistance, and excellent performance against contamination. However, recent studies have shown that composite insulators suffer from aging phenomena that deteriorates their

properties. It was found that aging of composite insulators causes a decrease in surface resistance and consequently, insulator surface would become more prone to contamination accumulation and water filming. The main causes of composite insulator aging are: dry band arcing, partial discharge, UV radiation, chemical reactions, etc. Among these, partial discharge was found to be the most severe factor affecting the aging process.

Partial discharge is considered to be the first alarm for composite insulator degradation. Therefore, it is of important to perform online detection of such degradation before the insulator is completely damaged. Partial discharge may be detected using many different techniques such as: acoustical sensors, Radio Frequency (RF) antennas and Radio Frequency Current Transformer (RFCT). Each sensor has advantages and disadvantages depending on the type of application it will be used for. In overhead lines, partial discharges are detected more efficiently using RF sensor due to its high signal to noise ratio and its high sensitivity compared with other sensors.

Although partial discharge detection is successfully implemented, it is not the only burden for utilities to stop aging of composite insulators. The most important thing after detecting partial discharge signals is to identify sources of partial discharge, so that proper corrective actions could be implemented to completely stop the aging process.

The purpose of this study is not only detecting partial discharges in outdoor insulators, but also to identify sources of partial discharge using artificial intelligence. In outdoor insulators, partial discharges have four main sources: surface discharge, corona discharge from energized end, corona discharge from dead end and combination of both corona and surface discharge happening at the same time. Using feed forward back propagation neural network, a clear distinction between the four classes of partial discharges is achieved with 96.3% recognition rate.

TABLE OF CONTENTS

LIST OF FIGURES

LIST OF TABLES

ACKNOWLEDGEMENT

I would like to express my sincere gratitude for my Professors Dr. Ayman El-Hag and Dr. Khaled Assaleh for their unlimited support until the competition of this work. Also, it is my pleasure to thank my parents, sister and brother in law who made this thesis possible through their continuous courage and support. Moreover, I would like to thank SIEMENS Transformer factory, specially Eng. Nilesh, for giving me the opportunity to use their lab. I don't want to forget my friends Yasser Saker, Abdulla Daher, Islam, Ahmed Moayyad, Khaled younis, Khaleel and Emad for being cooperative and sincere all the time.

CHAPTER 1: LITERATURE REVIEW

1.1 Introduction

Delivering power to customers with very low rate of interruption is a major concern to power utilities. Customers might vary from rural, where power interruption is not a serious problem, to industrial, where power interruption may lead to a huge loss of mass production. So, power interruption is a crucial issue and in some cases it is intolerable.

Power is delivered from the upstream (generation) to the downstream (distribution) using overhead lines (OHL) or underground cables (UGC). Due to its lower cost, OHLs are used more extensively than UGCs. The basic components of OHL are towers, conductors and insulators. Among these components, insulators have shown a great impact on the performance of OHL because of their frequent failure.

The main function of outdoor insulator is to provide sufficient isolation between live (high voltage) line and ground. Also, they have to mechanically support overhead lines. Their size will differ according to voltage level from few centimetres (low voltage level) to hundreds of centimetres (high voltage level).

Outdoor insulators have shown relatively higher failure rate compared with other network components. Insulator failure means that the insulator fails to isolate the line voltage from the ground. This failure might be due to mechanical reasons causing the line to drop or electrical reasons causing a flashover across the insulator. In transmission line, once an insulator fails, the circuit will be disconnected and this

will be interpreted by utility as a fault in the transmission line. Hence, it is important to have an adequate condition monitoring on outdoor insulator in order to predict the condition of insulators before it fails.

1.2 Outdoor Insulators

In distribution and transmission overhead lines, there are three main types of outdoor insulators: porcelain, glass and polymeric insulators. Porcelain and glass insulators are usually called ceramic insulators. On the other hand, polymeric insulators are usually called composite or non-ceramic insulators. The first insulators available in service since 1800 are ceramic insulators [1]. They have shown great capability of withstanding mechanical and electrical stresses. However, there are two main disadvantages that make them somehow not desirable for certain applications. One disadvantage is their heavy weight which leads to difficulties in insulator handling and tower design especially for extra high voltage lines (>100 KV) [2]. Another disadvantage is their poor contamination performance in which water filming is easily established and might lead, when progressing, to flashover. Therefore, there was a great need to improve the performance of the insulator under contaminated conditions. This leads insulator developers to the invention of non-ceramic insulators which first appeared in industry on 1970 [1]. These insulators have shown a superior performance against contamination conditions due to their water filming repellent property. Nevertheless, they suffer from degradation phenomenon that might lead to insulator failure due to various environmental, electrical and mechanical conditions.

Nowadays, utilities are widely using non-ceramic insulators especially in extra high voltage applications. However, the aging phenomena of non-ceramic insulators is not yet well understood and testing against contamination is not yet well standardized. Therefore, it would be of great importance to study non-ceramic insulators, their aging mechanism, and their aging detection using on-line monitoring methods.

1.3 Non-Ceramic Insulators

Each non-ceramic insulator consists mainly of three parts: the housing (sheath), core and end fitting as indicated at Figure 1-1 .

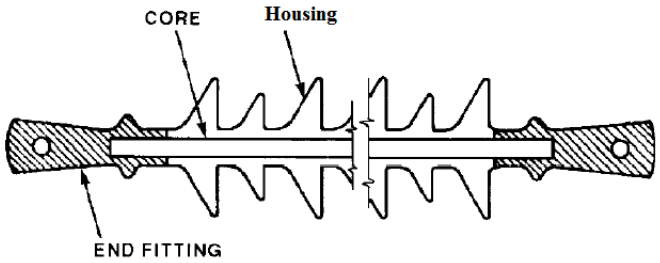

Figure 1-1: Schematic cross section of non-ceramic insulator

OHL cables are suspended using outdoor insulators. Due to the huge weight of OHL cables, composite insulators should be strong enough to withstand the mechanical stress of these cables. Therefore, composite insulator's core is utilized to add enough strength to the insulator, so that it can withstand mechanical stresses. The core is mainly made of fiber reinforced plastic (FRP) material. Another composite insulator component is the end fitting which has the role of fastening the insulator ends with the high voltage line and the grounded tower. It is made mainly from forged steel, malleable cast iron or aluminum alloy. The FRP core and end fittings are joined using compression methods [25].

Another component of non-ceramic insulator is the housing. It is the outer part of the insulator and it plays an important role in improving the insulator performance because of several advantages. One advantage is the enhancement of electrical strength of the insulator due to water filming repellent property of the surface material. This property is important to prevent leakage current and the any consequent dry band arcing. Another advantage of housing is the protection of the core against surrounding conditions such as moisture, contamination, sun light and corona. Moisture and contamination may asses the process of carbonization in the core which may lead to failure of the core and hence causing the line to drop. Also, sunlight will aid the degradation process of the core due to the continuous exposure to UV radiation especially in dry areas. Another reason of using the housing is to

protect the core from corona discharge which will lead to the formation of oxalic acids that cause the core to be brittle and when progressed it might cause the insulator to fracture [2], [8].

The housing material is made of various organic substances. Because of its excellent performance in regaining low surface energy (high water repellent capability), silicon rubber has been used in most of the application. The silicone atom has two main bonds, one bond is with organic chain and the other bond is with oxygen. The silicon rubber material is called polydimethylsiloxane(PDMS), polydiphenylsiloxane (PDPS), or polydivenylsiloxane (PDVS) based on the corresponding organic chain methyl, phenyl, or vinyl; respectively [3].

The main concern in non-ceramic insulators is the aging of their organic material (the housing). Therefore, it is important to have a deep understanding about the aging forms and the aging process.

1.4 Aging Forms

There are different forms of aging based on insulator aging process. The main aging forms are chalking, cracking, corona cutting and puncture.

A. Chalking

Chalking is a white powder appears on insulator surface. It is mainly the fillers within polymer structure. The main cause of chalking is UV radiation and electrical activity which expose fillers outside on the surface of the insulator. This phenomenon mainly appears in ethylene propylene rubber (EPR) insulators [7].

B. Cracks

Due to electrical stress, shallow cracks appear on the surface of the insulator with a depth of less than 0.1 mm. This type of cracks is called crazing. When crack depth is more than 0.1 mm, these cracks are called alligatoring. This type of cracks ultimately affects contamination performance of the insulator and might expose the fiber glass rod to the surrounding environment [7].

C. Corona cutting

Due to bad insulator attachments, corona discharge will start to appear at the insulator ends towards the last shed causing insulator cutting or what is called corona cutting. This phenomena causes severe electrical and chemical degradation to the insulator [7].

D. Puncture

Due to impurities within the housing or rod material, internal discharges will be initiated. This will be followed by progressive discharges that will eventually cause puncture to the housing or rod material [7].

E. Tracking

This phenomenon was observed after leakage current activity where tracks were formed on the insulator surface. These tracks contain high concentration of conductive carbon. This will cause a severe deterioration to the insulator by reducing its resistance [7].

F. Erosion

Due to leakage current energy, it will cause a loss of housing material in some localised location of more than 1 mm causing material erosion. This phenomenon reduces the protection against ingress of water to the rod. This phenomenon usually doesn't cause insulator failure unless it is so severe such that water could reach to the rod [7].

1.5 Aging of Non-Ceramic Insulators:

Because of the organic nature of non-ceramic insulators, degradation of the insulator is inherent. Insulator degradation is caused mainly by two factors: environmental and electrical factors. Environmental factors include temperature, UV radiation, rain and pollution. On the other hand, electrical factors include partial discharge and leakage current. In each factor, insulator degradation starts by losing some of its organic properties (hydrophobicity). The focus of the coming sections will be about the effect of electrical factors, in degradation process.

1.5.1.1 Loss of Hydrophobicity

Hydrophobicity is defined as the ability of the insulator surface to repel water and prevent the formation of water filming [4]. This property is important to increase the leakage distance of the insulator by increasing the surface resistance. Hydrophobicity is related to critical surface tension. The magnitude of hydrophobicity is inversely proportional to the surface tension [2]. Because the polymers have very low surface tension their surface hydrophibicity value is relatively high.

In service polymer insulators experience various environmental and electrical factors that might affect the degree of hydrophobicity of the insulator surface or might even completely change it to be a hydrophilic surface (low resistance surface). These factors are contamination, UV radiation, moisture, and electrical discharge [2]. It was found that these factors cause an increase in oxygen level at the surface of the insulator which might be due to two main reasons. The first reason is due to the reorientation of the polymer molecules to have the oxygen atoms directed outward instead of inward. The second reason is due to the reaction between the oxygen atoms in the environment and the polymer molecules due to electrical discharges [4], [5], [6]. It was found that UV radiation, contamination and moisture has minor effect on the silicone rubber surface hydrophobicity unlike other types of polymer insulator.

1.5.2 Degradation due to leakage current

After losing hydrophobic property of insulator surface, water filming will be created causing the surface resistance to decay. Consequently, leakage current will flow across the water layer. Narrow parts of this layer will have high current density leading this water portion to evaporate and therefore leading to the formation of dry bands. The line voltage will be applied across dry bands leading to significantly increase the electric field in these areas. Once reaching a break down field, an arc will be developed across the gap. The current of this gap depends on many factors such as wind, resistance of water layer and resistance of the insulator surface. The magnitude of the arc is only a few milliamps. The higher the resistance of the insulator surface, the more rapidly the arc could be extinguished [2] and [4].

Thermal degradation of Silicone Rubber (SiR) insulator that contains Alumina Tetra Hydrate (ATH) and silica fillers due to arcing conditions was demonstrated in [3]. It was found that the energy of dry band arcing can increase the temperature on localised spots on the insulator surface to be sufficient for polymer degradation. It was observed that the degradation starts when the arcing current exceeds 10 mA [3]. When arcing develops, it causes leakage current to increase, surface to depolymerise, polymer structure to be changed due to crystallization of silicon chain, and polymer fillers to be clustered. As a consequence, tracking and/or erosion will take place and gradually the insulator will experience complete failure [17].

Dry band arcing was found to be correlated with LC harmonics. An extensive study of LC in composite insulators during clean fog tests was carried out in [27-30]. It was noticed in LC measurement that there was a deformed sinusoidal shape of LC during the experiment. There were three deformed shapes that have large number of fifth and third harmonics. This was attributed to the formation of non-linear current density on the surface of the insulator. This can be modeled as linear resistor in parallel with a capacitor for the un-wetted region, as non-linear resistor for the wetted region, and as capacitor-resistor combination to represent the rest of the insulator. In another test performed by [21], high frequency component (10KHz-500 KHz) and low frequency components (50 Hz) were measured. A good correlation was established between arcing and high frequency components. Another test was done to measure LC on a post ceramic insulator placed in a fog chamber [22]. It was also found that when the arcing increases, the total harmonic distortion (THD) increases as well.

LC measurement stations are distributed in many places for both field and lab investigation. This is done especially for insulators near coastal areas where dry band arcing is more frequent. During a slat storm, the peak value of LC was measured for four different insulators: SiR insulator with a creepage distance of 3590, SiR insulator with a creepage distance of 2244, porcelain insulator with RTV coating [18]. The measurement showed a peak leakage current of less than 1 mA for SiR insulator with larger creepage distance and porcelain insulator with RTV coating; however, values

of 20-30 mA of leakage current was measured for the other two insulators. Another measurement was done by measuring peak value of leakage current on two different non-ceramic insulators (EPDM and SiR) placed on a highly polluted area [19]. It was noticed peak LC measured was higher in SiR; however, the EPDM insulator surface was more aged than the SiR insulator surface. The peak value of LC was correlated with the degree of aging [20]. It was found that for LC peak values of more than 4 mA, visible erosion will be observed.

Though LC detection is a very important indicative parameter for ceramic insulator performance, it might be not that helpful in condition monitoring of non-ceramic insulators before degradation. Because composite insulators are commonly known by their hydrophobic property, any leakage current detected means that the insulator has lost its hydrophibicity to a high extent. The author at [9] conducted a 500KV accelerated aging test on non-ceramic insulator. It was observed that the degradation of the insulator happened without detection of LC even though the detection threshold was held at 500 pA [8]. Therefore LC measurement may not be a good indicator to predict insulator aging in early stages so that a proper corrective action could be taken to prevent insulator aging and consequence failure. Instead, it was concluded in [8] that PD detection could be a better indication of insulator aging.

1.5.3 Degradation due to partial discharge

PD is one of the main aging mechanisms of composite insulators. It is initiated due to electric field enhancement caused by water content on insulator surface (surface discharge) or due to metallic edges on both insulators ends (corona discharge). It was stated in [26] that partial discharges interact with atmosphere's moisture leading to the formation of acidic liquid by products that might cause chemical reactions to take place between these acids and polymeric material. Also, the energy released by the partial discharge (in a microscopic level) might be considered as a localized source of heat that releases energy possibly capable of breaking the weakest bonds in polymer matrix.

Ivans [14] was among the first people who verified the effect of PD on the surface of non ceramic insulators. He reported that the electric field enhancement on the surface of the insulator due to water droplet depends on the size and number of droplets. Moreover, PDs in condensation condition were studied and found that the threshold field for PD inception was 3-3.5 kV/cm. However, Ivans experiment was conducted using standardized testing method which is not reliable for online monitoring.

Insulator surface pollution and wetting plays an important role in increasing PD activity. A polymer insulator in many different conditions was tested in [12]. It was confirmed that there was no PD detected in dry clean or polluted insulator. However, when wetted, partial discharge patterns clearly appeared. Therefore, insulator wetting is the main factor that controls the PD activity on the surface of the insulator.

To verify the wetting factor, silicone rubber insulator was examined with fixed pollution level and variable humidity level [12]. It was found that the amplitude and time length of PD pulse are enhanced with increasing humidity level. Also, it was noticed that the frequency content of PD is in the low range (2-6 MHz) for high humidity level (above 90%), and in the high range (6-25 MHz) for lower humidity level (60-80%). Moreover, the rise time of the PD pulse is proportional to the humidity level.

While fixing the humidity level, pollution variation and its effect on PD activity was also verified by [12]. The pollution level was varied between 0.06-0.25 ESDD and the humidity was kept constant at 98%. At highly polluted condition (0.12-0.25 ESSD), it was observed that the PD pulse is large and it's happening at series of consecutive pulses. Also, it was observed that low frequency contents of PD (1-6 MHz) increases with high pollution level. It was also noticed that PD repletion rate decreases with increasing pollution level.

Moreover, several experiments were conducted to study the effect of water droplets on electric field along non ceramic insulator. Mainly water droplets could be formed in two locations along the insulator surface: the sheath and the shed. It was

observed that the electric field enhancement in the sheath is much higher than the shed. Moreover, the larger size water droplet will enhance the electric field in its vicinity more than in smaller size water droplet [9], [13], and [14].

Another form of PD is corona discharge. Gorur and Moreno tested HTV-Silicone Rubber samples by exposing them to corona discharges under high humidity conditions with and without mechanical stressing in a corona test cell. Constant AC voltage (7.2 kVrms), temperature (40°C) and relative humidity (>85%) were kept throughout the 500 hour corona exposure time. Samples showed not only a total whitening but also formation of cracks on the surface area exposed to corona. Corona discharges combined with moisture give rise to chemical reaction that may strongly interact with the polymer housing of non-ceramic insulator, thus promoting degrading mechanisms on the polymer surface initially, and eventually progressing toward the polymer volume [13] .

1.6 Online PD detection methods

When a PD signal is emitted, it will be radiated in the form of light, acoustic emission (AE), vibration & electro-magnetic (EM) signal. There are mainly two methods to detect PD signals: impedance detection method &secondary detection of other quantities (EM and AE waves) [23]. Impedance detection method is a standardized method (IEC 60270) and is most widely used by factories. Using this method, the phase, compared with applied voltage, and polarity of PD signal will be identified. The most common advantages of this method are the possibility of calibration, the easiness of reproducing the measurements and the standardization of this method. On the contrary, this method cannot be used in the field because of transportation, installation and noise problem [23].

In secondary detection methods, many techniques are proposed to detect PD waves such as EM, and acoustic emission (AE) techniques. In the former method, when the electric field increases, partial discharge process will be initiated. When PD is initiated, it is accompanied with movement of electrical charges. If these charges are moving with accelerated speed, EM waves will be radiated from PD pulses

towards all direction. The main difficulties that face this method are the low power of EM wave emitted by PD signal and the attenuation of EM wave with distance. One of the main sensors used for EM detection is UHF sensor. This sensor is used widely in gas insulated switchgear (GIS) application to detect EM wave due to PD pulse in breaker insulators, spacers and cable termination [24]. This technique is also subdivide into two main topologies: narrow band detection and wide band detection. In the former method, the resolution of the detected signal can be narrowed using the spectrum analyzer. In the later method, the EM wave can be viewed as time domain signal by an oscilloscope using wide-band-pass filter. The most favourable advantage of this technique is the disturbance noise tolerance and high sensitivity that reaches to 1 PC. On the other hand, one of the main disadvantages is signal attenuation with distance. Another drawback is that it's not possible to calibrate it because the sensor output depends on discharge location [23].

The AE detection method is now widely used high voltage application. It is used to detect the behaviour of foreign particles in GIS and PD location in transformers. In GIS application, it is observed that sensitivity of AE signal attenuates with distance. Also, the AE measurement doesn't give a comparative indication about the amount of charge available. For oil-immersed transformer, the PD vibration is converted into charge transfer using piezoelectric element and it has a spectrum range from tens to hundreds KHz. The sensitivity of AE sensor is much lower than the conventional IEC method because of 2-20% decay of the signal during propagation to reach 500 to several thousands pC. It is recommended to use other methods along with this method to validate results [23].

Another detection technique based on using array of antenna was suggested in [10]. This radio frequency antenna was fixed on top of a vehicle and used to trace defected insulators. It was noticed that low level radiated field from the defected insulator is capable of degrading radio and TV channels.

Another technique was used by [11] to detect PD signals. The detector used was Rogowski coil which was clamped on the ground strap of the tested specimen. The use of fibre optic cable and corona free transformer was very important to avoid

any interference. The author didn't mention any problem from this technique when he used it online around the ground strip of 220KV CT.

1.7 Thesis Objectives and Contributions

It is clear from literature that partial discharge is the main cause for non-ceramic insulator degradation. So, it is essential to monitor these insulators against any PD activity that might initiate the degradation process. In utilities, detection of PD incidents in outdoor insulators is a first step for insulator diagnosis. The following steps are the most time consuming to find the source of defect and might require unnecessary shutdowns. In this thesis, PD discharge will not only be detected, but also different types of defects will be identified. There are four main types of defects to be distinguished: surface discharge due to contamination, corona from energized end due to bad end fitting, corona from dead end due to bad end fitting, and combination of both corona and surface discharge.

1.8 Thesis Outline

In the first chapter a literature review about outdoor insulators will be introduced. The focus will be on Non-ceramic insulators, and their aging mechanism. After that aging detection using online monitoring methods will be introduced and concluded by thesis objective. In chapter two, methodology and experimental setup are illustrated. In chapter three, PD detection using conventional method, implemented in SIEMENS factory, is demonstrated. In chapter four, methodological comprehensive results will be presented. Finally, in the fifth chapter, a conclusion will be drawn based on the presented results, application and future work will be proposed.

CHAPTER 2: EXPERIMENTAL SETUP AND RESEARCH METHODOLOGY

2.1 Experimental Setup

This experiment is mainly done to generate and capture different PD signals. The experimental setup consists of: PD sensor (RF antenna), 15 KVA step up dry type transformer (220V/20KV), amplifier, high voltage probe (1/1000 ratio), digital four channel oscilloscope (60 MHz-1Gs/second) and SiR insulator specimen.

The insulator specimen is fixed between two parallel aluminum plates enclosed by a transparent reinforced plastic box. One plate is connected to the step up transformer and the other plate is grounded using copper strip. The length of the insulator was chosen to be 4 and 1cm. The insulator length was chosen due to limitation of the step up transformer. This limitation was raised because of non-free partial discharge nature of transformer. It was observed that the transformer confirms a partial discharge free nature up to 6.6 KV. However, beyond 6.6 KV, the transformer starts to emit PD signals from the winding. The high voltage probe was used to monitor the voltage at the secondary of the transformer using oscilloscope. The experimental setup is shown in Figure 2-1.

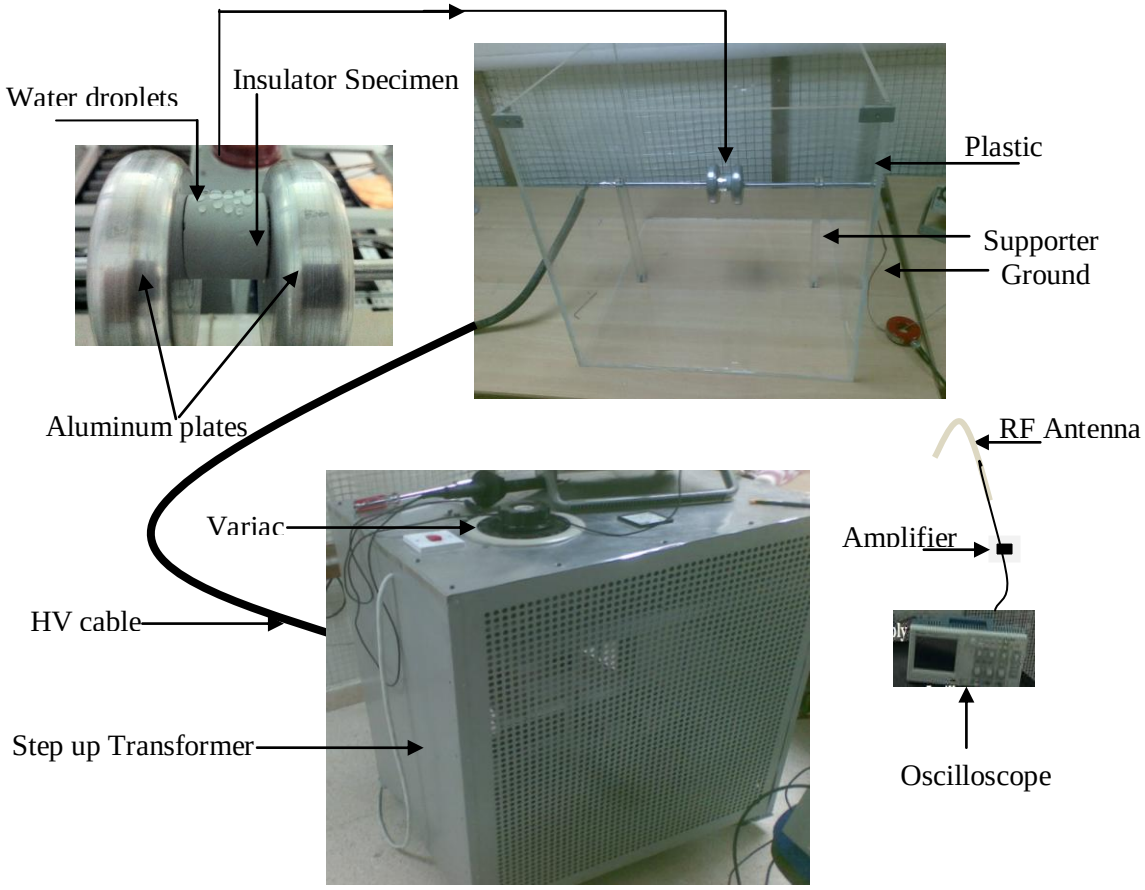

Figure 2-1: Experimental Setup

2.2 Research Methodology

The research methodology is composed mainly of four parts: signal generation and acquisition, feature extraction, feature selection and classification using artificial neural network. Signal generation will be done using the experimental setup. Many cases will be examined and PD signals will be acquired and saved. There are mainly four cases to be studied: surface discharge, corona from energized end, corona from dead end and combined PD. Then, important features will be extracted from each PD signal. After that, feature selection will be done to reduce the dimensionality of the extracted features. Finally, the selected features will be fed to an artificial neural network to classify between different classes of partial discharge. A diagram of research methodology is shown in Figure 2-2.

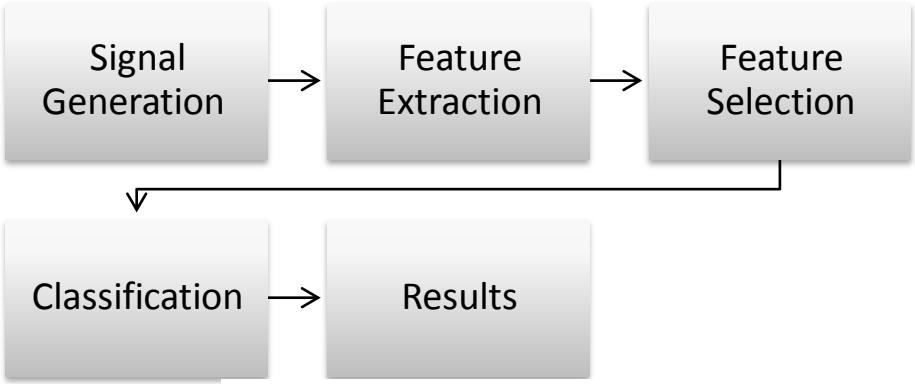

Figure 2-2: Research methodology

2.2.1 Signal Generation

In this section, four different models to generate PD signals are demonstrated. It should be noticed that each model represent a separate class. Also, switching signals will be generated which represent a model for non PD signals class.

The first model is utilised to generate surface discharge signals. The insulator specimen will be tested for different conditions. Water droplets are placed on the surface of the insulator as a main source of PD to simulate surface discharge on real insulators due to contamination. Also the effect of water droplet location and the effect of water droplet grouping will be investigated. Water droplet grouping will simulate condensation which is the most severe case of PD. The model that will be used is shown in Figure 2-3.

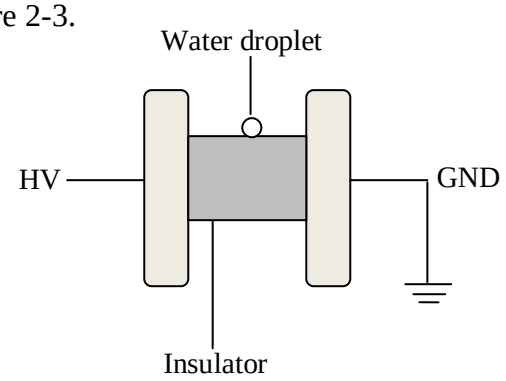

Figure 2-3: Proposed Model to study to surface discharge due to water droplets

Another model to be investigated is PD due to hardware problem. Hardware discharge can be simulated using sharp edge placed at the energized and dead end. This sharp edge will intensify the electric field around it causing corona to be generated. Model of corona from energize and dead end is shown in Figure 2-4 (a)

and Figure 2-4 (b) respectively. For each case, many samples will be generated and recorded.

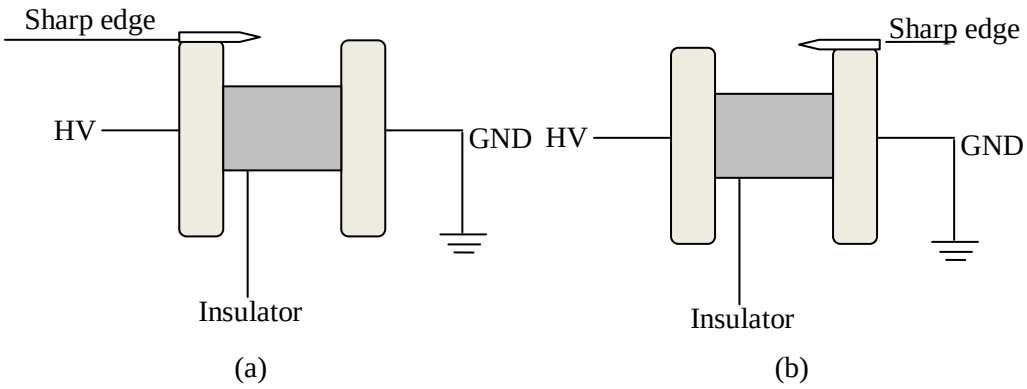

Figure 2-4: (a) Proposed Model to study corona from energized end
(b) Proposed Model to study corona from dead end

The last PD model to be studied is when surface discharge and corona are happening at the same time. This case is experimented using the model shown in Figure 2-5.

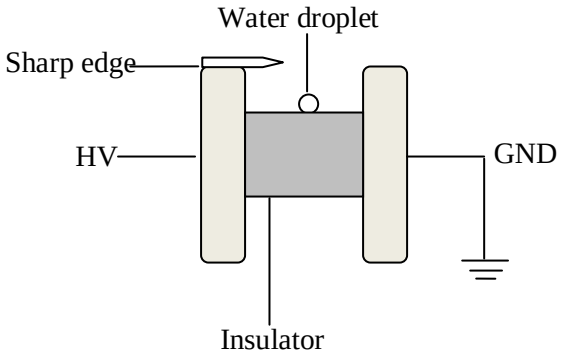

Figure 2-5: Proposed model to study corona and surface discharge happening at the same time

Moreover, it is important to distinguish between PD and non-PD signals detected by the RF antenna. One example that will be studied is the switching signal. The switching signal will be generated using the ON/OFF switching of the transformer.

2.2.2 Feature Extraction:

After signal generation an acquisition, it important to extract some important features such as statistical and FFT features. These features will be used later on by feature selection and classification section.

2.2.2.1 Statistical Feature Extraction

It is of great importance to study the correlation between the PD defects and their statistical patterns. A set of statistical features such as kurtosis, skewness, median, mean, standard deviation & variance will be calculated. Each feature is studied separately and the effect of combining them is examined.

Mean: It is the central value of the function at each half cycle.

Standard Deviation: It describes the width of the function around its mean. If the standard deviation is low, this means that the function data is very close to its mean, while a high standard deviation indicates that the function data spread over a wide range.

Skewness: It describes the degree of asymmetry of the function. A zero value skewness indicates that the function is symmetrical. If the function is asymmetrical with a tail pointing towards the left, the skewness of the function is negative. While a function having positive skewness will have a tail pointing towards the right [28].

Kurtosis: It is a measure of degree of sharpness of a distribution compared to a normal Gaussian distribution. Zero kurtosis indicates a normal distribution. While positive kurtosis indicates a sharper distribution and negative kurtosis indicates flatter distribution [28].

2.2.2.2 Fourier Transform Feature Extraction:

Fourier transform is a mathematical tool to extract the frequency component of a time domain signal. This transformation is based on a basis function that are bansed on complex sinousoids. The frequency content of the acquired signal (partial discharge) is very important for signal analysis and recognition. Since the acquired signal is digitized, the frequency spectrum is found using discrete Fourier transform (DFT).

To find DFT of a signal, it should be discrete and periodic. The acquired PD signal is discrete by the digitization done by the oscilloscope. It is also periodic, when assuming that the detected signal is a one period of an infinitely long periodic signal. The DFT of a given time domain sequence $x_n\{n = 0, 1, 2, \dots, N-1\}$ is given by Eq. 2-4:

$$\mathrm{X_k} = \sum_{\mathrm{n=0}}^{\mathrm{N-1}} \mathrm{x_n} \mathrm{e}^{\frac{-2\pi \mathrm{i}}{\mathrm{N}}\mathrm{kn}} \qquad \text{Eq. 2-1}$$

To reduce the computation time in computer environment, fast Fourier transform (FFT) is used instead of DFT. The number of operation done by DFT is $O(N_2)$, while in FFT it performs only $O(N\log_2 N)$ operations [27].

2.2.3 Feature Selection:

After features extraction, feature selection can be done to reduce the dimensionality of the feature vector and to select the more relevent features. Feature seletion is done using two methods: heuristic method and stepwise regression method

2.2.3.1 Heuristic Feature Selection:

Heuristic method is an iterative method used to maually select more relevant features. Firstly, the feature vector is segmented into bands (A) of equal length. Then, each segment is tested and trained using the NN. After that, according to band's score and by inserting certain thresholds, bands (A) with highest score are selected for further analysis. The selected bands are further segmented into smaller bands (B) of equal length. And then, each band is tested and trained using the NN. Then the highest score bands will be selected based on certain threshold. This process is continued until we reach a band length of three samples. The result of this analysis is a set of samples that can be used to form the final feature vector.

2.2.3.2 Using Stepwise regression

After feature extraction, it is noticed that the dimensionality of the feature vectors is large and this might cause an excessive training and classification operations. Therefore, stepwise regression is used as an iterative tool not only to reduce the dimensionality of the feature vector but also to select the most significant information within the feature vector. In this study, we have n number of variables $x_1, x_2, ..., x_n$ (PD samples) and a response variable y (PD class). Initially, one variable regression model will be made using the variable that has the highest partial F-statistic and highest correlation (lowest p-value) with the response variable *y*. Then the remaining *n*-1 variables will be tested such that variable that generates the highest partial F-statistic, given that it is larger than f_{in} random variable for adding variable to the model, will be added to the model [30]. Therefore the partial F-statistic for the second variable is given by:

$$f_2 = \frac{SS_R(\beta_2|\beta_1,\beta_0)}{MS_E(x_2,x_1)} \qquad \text{Eq. 2-2}$$

Where β_i is the regression coefficient for i[th] variable. And $SS_R(\beta_2|\beta_1,\beta_0)$ is the regression sum of squares casued by β_2, and β_1,β_0 are initially in the model. And $MS_E(x_2,x_1)$ referes to the mean square error of the model when containing both

$$f_1 = \frac{SS_R(\beta_1|\beta_2,\beta_0)}{MS_E(x_1,x_2)} \quad \text{Eq. 2-3}$$

variables x_2 and x_1. The partial F-statistic can be found generally using the following equation:

$$f_j = \frac{SS_R(\beta_j|\beta_0,\beta_1 \ldots \beta_{j-1},\beta_{j+1} \ldots \beta_n)}{MS_E(x_j,x_1)} \quad \text{Eq. 2-4}$$

After adding x_2 to the model, the condition of removing the variable x_1 from the model should be examined. This is done by finding the F-statistic of the variable x_1. If the evaluated F-statistc is less than f_{out} random variable, the variable x_1 will be removed.

This procedure continues to add or remove variables from the model and stops when there is no sufficient condition for removing or adding[30]. Stepwise regression is employed using MATLAB envornment. The default values for f_{in}, and f_{out} are 0.05 and 0.1; respectively. Another terminology of entering and removing terms from the model is by observing the p-value of each term. If a term outside the model has p-value less than f_{in}, it will be entered to the model. On the contrary, if a term inside the model has p-value larger than f_{out}, it will be removed from the model. Each time a term is removed or added to the model, p-values of all the terms will be updated.

Although stepwise regression provides a very good estimate for the required model; the selected terms to be in the model might carry significant information. This is mainly due to probabilistic errors in retaining repressors [30]. This is clearly shown when changing initial entering term, which will result in different model for different initial term. Therefore, it is important to examine several models before reaching to a final conclusion. In this study, several models were examined using different f_{in} threshold. The f_{in} threshold is varied using values lower than or equal to 0.05. Two methods are used to generate different models based on varying p-entering threshold. The first and second methods are named Frequency Repetition Based

Model (FRBM), and Variable P-value Based Models (VPBM). Both models are generated by varying the p-value threshold.

Using FRBM, by varying p-entering threshold, n different models will be created and saved in A_i. After that, among these n models, frequency repetition search will be impleneted.

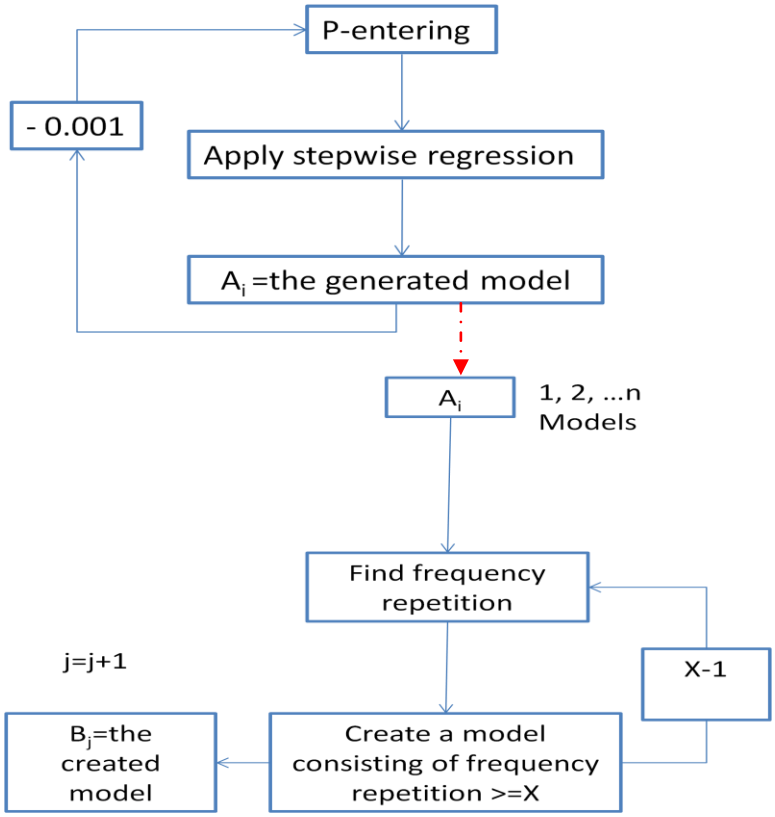

Figure 2-6: FRBM algorithm

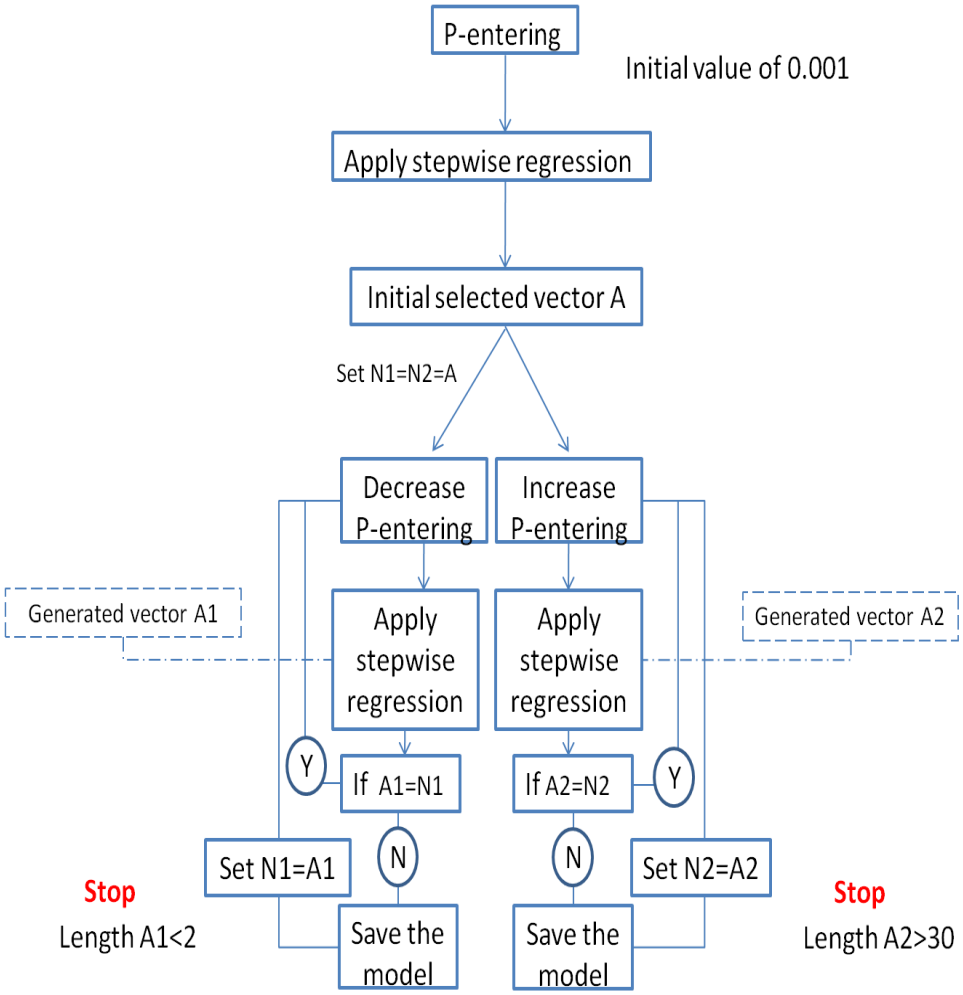

Figure 2-7: VPBM algorithm

Then the first model (B_j) will be created by combining frequencies repeated greater than or equal to X times. The second model will have more variables by decreasing the repetition rate by -1. This process continues untill repetition rate X reaches 1. The algorithm is shown in Figure 2-6.

Using VPBM, start the process by p-entering threshold that generates moderate model length (5-15 features). This will be an initial model and will be saved in vector A. After that two new vectors will be initialized and will N_1=N_2=A. Then start to decrease and increase p-entering threshold and save the generated model in A1 and A_2; respectively. If the generated model is identical to the initially generated model N_1 and N_2, p-entering threshold will varied and the process will start again. If

the generated model is new, save the model. The algorithm of this method is shown in Figure 2-7.

2.2.4 Artificial Neural Network

After creating different models using feature selection techniques, these models will be used to train and test the NN. If the mapping between two types of signals is linear, normal linear classifier can be used to discriminate between them. However, if these signals have non-linear relationships, more complex classifier should be used to discriminate between them such as neural network (NN). The proposed technique to be used for ANN is based on back propagation algorithm. Artificial neural network is widely used in modern engineering applications. The main purpose of using ANN is the non-linear relationship between input (PD signal) and the output (PD source).

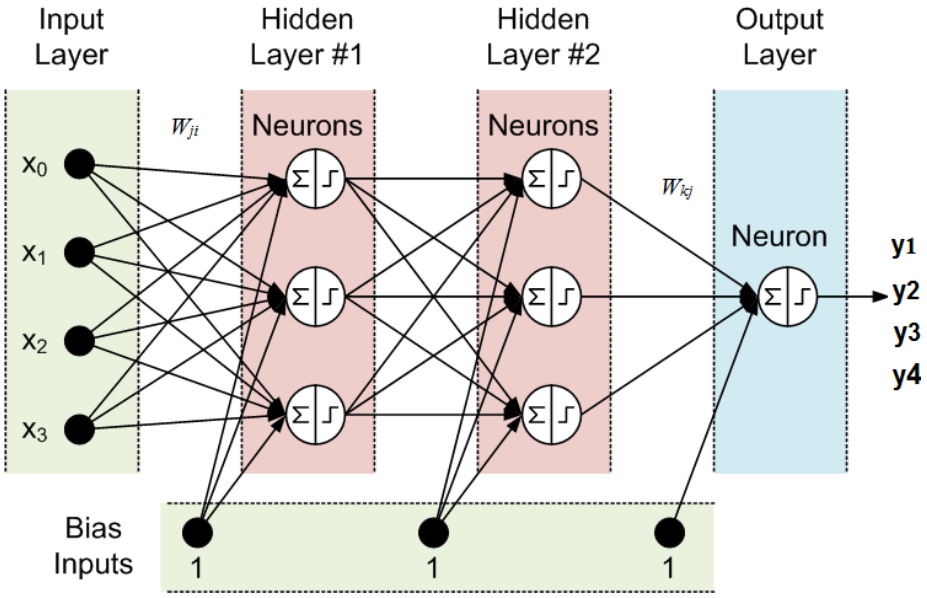

Figure 2-8: Three layer neural network

The neural network structure utilized in this study is made of 3 layers: one input layers, two hidden layers and one output layers as shown in Figure 2-8. Each layer is made of number of neurons and each one is made up of input, bias, activation function and output. Each input x_i will be weighted by W_{ji}, a weight between the i^{th} input and the j^{th} hidden layer. After that it will be summed with a bias b and multiplied by the activation function *f*. The activation function used in neuron model is tan-sigmoid (Tansig) which has a range between -1 and +1 as shown in Figure 2-9 [15].

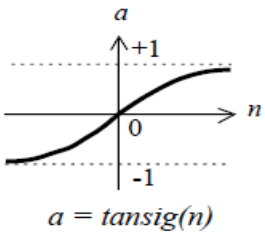

Figure 2-9: tan-sigmoid activation function

Then the hidden layer will calculate its net activation as the following equation:

$$net_j = \sum_{i=1}^{n} x_i w_{ji} + w_{j0} \quad \text{Eq. 2-5}$$

Where w_{j0} is the weight between the jth hidden layer and the bias and n is the number of features.

The net activation of the output hidden layer is calculated using the following equation:

$$net_k = \sum_{i=1}^{N} y_j w_{kj} + w_{k0} \quad \text{Eq. 2-6}$$

Where y_j is the output of the hidden layer which a function of the net activation, w_{k0} is the weight between k^{th} output and bias, N is the number of neurons in the hidden layer The output layer z_k is a function of its net activation function. The output of the NN can be expressed in terms of inputs and weights as shown in the following equation [15]:

$$z_k(x) = f\left(\sum_{i=1}^{N} w_{kj} f\left(\sum_{i=1}^{n} x_i w_{ji} + w_{j0}\right) + w_{k0}\right) \quad \text{Eq. 2-7}$$

2.2.4.1 Neural Network Training

Once the NN weights and biases have been initialized, the network is ready for training. During the training process, the biases and weights will be adjusted iteratively to achieve minimum network performance function. The used network performance function is the mean square error function (MSE) which is the average squared output between the actual and target output [29].

The gradient decent algorithm is implemented using two modes: incremental mode and batch mode. In the former mode, after each input is applied to the network, the gradient is computed and the weights are updated. In the later mode, all the inputs are fed to the network before the weights are updated. In this work the batch mode will be used [29].

There are mainly two batch training modes: gradient decent, gradient decent with momentum. The former has the steepest decent function where biases and weights are updated in the direction of the negative gradient of the performance function. Compared with gradient decent batch, gradient decent with momentum provides faster convergence. Momentum acts like a low pass filter by ignoring small features in the error surface [29].

For faster modes, a modification is done on the previous modes to form gradient decent algorithm (GDA) which is used in this work. This technique is based on variable learning rate back propagation. During learning process, the learning rate will change adaptively such that the learning step is kept as large as possible while keeping the learning stable. This learning process follows certain procedure. First, initial error and output are calculated. Then, biases and weights are calculated at each epoch using the current learning rate. After that, network output and error are calculated again. If the new error is more than the old error, the current weights and biases will be discarded and the learning rate will be decreased. However, if the new error is less than the old error, the current weights and biases are stored and the current learning rate will be increased [29].

The training error is the sum of the squared difference between the desired and the actual output of the network [15].

$$J(w) \equiv \frac{1}{2}\sum_{k=1}^{c}(t_k - z_k)^2 = \frac{1}{2}\|t - z\|^2 \qquad \text{Eq. 2-8}$$

Where J(w) is the training error, t and z are the target and actual output respectively, c is the output length and w is all the weights in the network.

CHAPTER 3: RESULTS

This chapter include two main sections. The first section is about PD detection using conventional methods. This section elaborates results obtained by a factory experiment to do some PD measurement using the conventional method. The second part of this chapter is PD detection using online methods (RF antenna). This part presents the bulk results of this thesis.

3.1 PD Detection Using Conventional Method

It was important to experience PD patterns of each class using the conventional PD detector. An experiment was held in SIEMENS factory to collect some PD measurement of each class. The PD detection was based on IEC-60270.

3.1.1 Detection Method

The PD measurement circuit consists of step up transformer (Tr), specimen under test (Ca), measuring impedance (Zm), noise blocking filter (Zn), coupling capacitor (Ck) and PD measuring instrument (Mi). The PD measuring circuit is shown in Figure 3-1 [16].

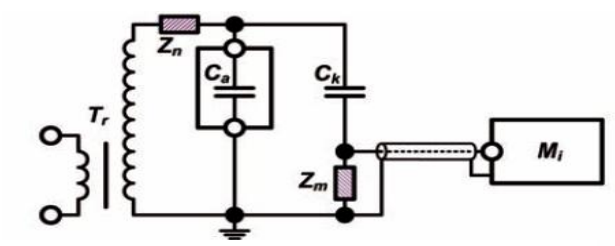

Figure 3-1: PD masurement circuit [16]

The main purpose was to measure the apparent charge (qa). This instrument was equipped with, matching unit attenuator, band pass filter amplifier, A/D converter, acquisition unit, display unit, memory unit and control unit. The detection diagram is shown in Figure 3-2 [16].

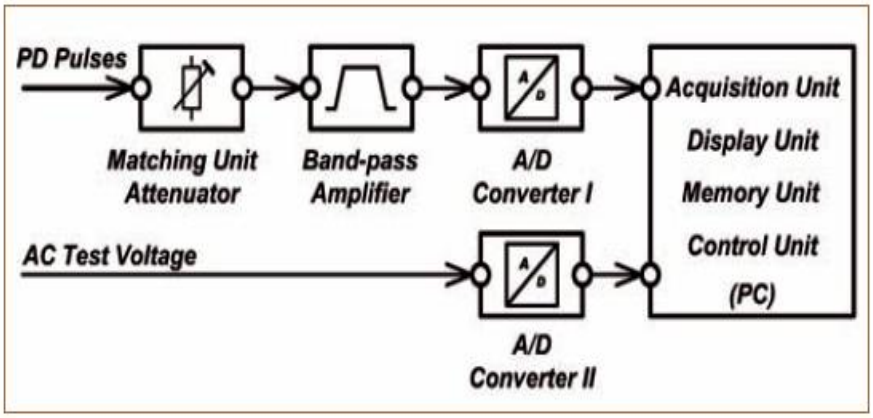

Figure 3-2: PD detection diagram [16]

A. Corona from energized end:

A sharp needle was placed in the energized end of the 4cm long insulator. The voltage was increased slowly until a PD inception was reached at 3.1 KV. It is clear from Figure 3-3 that PD pulses are concentrated on the fourth quarter of the applied voltage. However, as the voltage increased PD pulses started to repeat more frequently. Also, PD pulses started to appear on the third quarter of the applied signal.

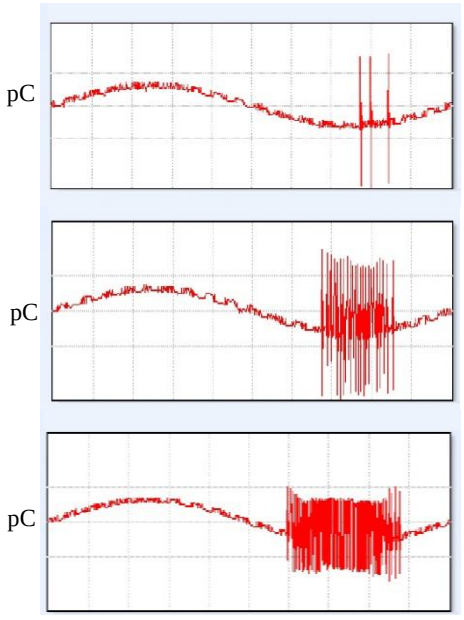

Figure 3-3: Corona from energized end

B. Corona from dead end:

A needle was placed on the grounded end of the insulator. It is clear that the inception voltage is much higher than the previous case. Figure 3-4 shows that PD pulses were more concentrated in the first and second quarters of the applied signal. When voltage was increased to 5.7 KV, the PD pulses started to appear on the third quarter; and upon further increase of voltage, new PD pulses appeared on the fourth quarter as well.

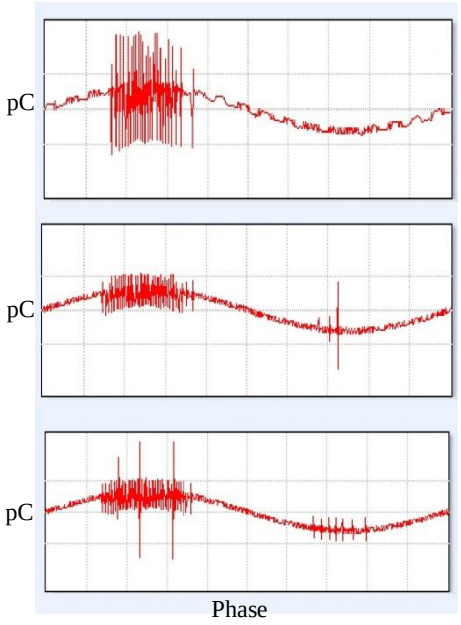

Figure 3-4: Corona from dead end

C. Surface discharge due to water droplet:

It was noticed that surface discharge is the most difficult type to be generated. The surface of the insulator was non-uniformly wetted with water droplets to simulate surface discharge. The PD pulses appeared in the first quarter of the applied voltage as shown in Figure 3-5.

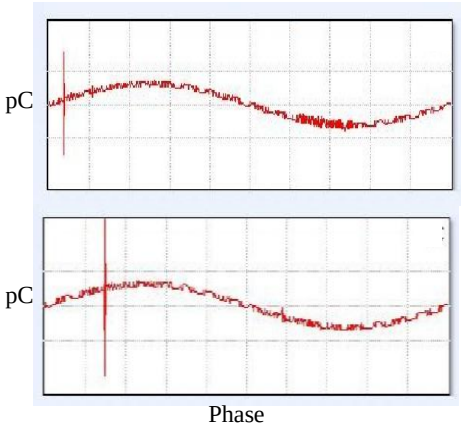

Figure 3-5: Surface discharge

D. Corona and surface discharge :

To investigate the effect of having both corona and surface discharge at the same time, sharp needle was placed on the energized end and water droplets were placed along the surface of the insulator. It is quite clear from Figure 3-6 that PD pulses are distributed in the first and third quarter of the applied signal. The PD inception was at 5KV with only two pulses; and when the voltage was increased the number of pulses also increased.

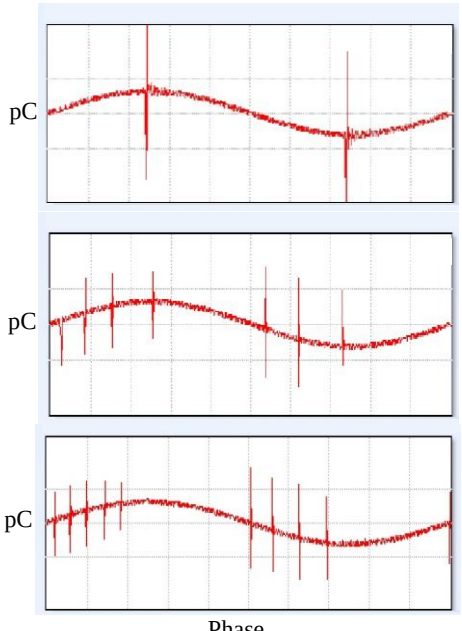

Figure 3-6: Corona and surface discharge

Table 3-1: Quarter of PD pulse occurrence

	Quarter 1	Quarter 2	Quarter 3	Quarter 4
Corona from energized end			Yes	yes
Corona from dead end	Yes	yes		
Surface discharge	Yes			
Corona and surface discharge	Yes		Yes	

Figures 3-3 to 3-6 show that each PD type occures at certain quarter (phase) of the applied voltage. It is also noticed that corona from dead end has the highest charge compared with other types. It is clear that this method can be used to distinguish between different PD sources. Unfortunately, this method can not be used online because of several problems such as: transportation difficulties, noise control problem, and calculation of the required coupling capacitance needed for proper measurement. In contrast, the proposed method of online PD detection using RF antenna is much simpler in terms of easy handling and transportation.

3.2 Experimental Results of the Proposed Method

Experimental results are mainly composed of two parts: partial discharge source identification and non-partial discharge source identification. In the first part, different sources of partial discharge occurring in composite insulators will be investigated. The four PD sources are: corona from the energized end, corona from the grounded end, surface discharge due to water droplets, and simultaneous corona and surface discharge. It is important to discriminate between these different sources of PD so that proper corrective action can be implemented.

The second part discusses the identification of non-partial discharge signals available in the atmosphere. It is important to discriminate between PD and non-PD signals to avoid false alarms in our system. An example of non-PD signal is the switching signal from nearby sources. Because the switching signal lies in the RF domain, the RF antenna detects the switching signal. Therefore, it is necessary to identify those non-PD signals to distinguish them from normal PD signals.

3.2.1 Partial Discharge Source Identification

After capturing partial discharge signals using the experimental setup, several steps were performed to achieve final results and these steps are: pre-processing, feature

Table 3-2: Surface discharge Observation

Inception voltage	Location			Grouping	Insulator size (cm)
	HV	Mid	Gnd		
400 V	Y			Y	2.5
880 V	Y			Y	2.5
923 V	Y			Y	2.5
1 KV		Y		Y	2.5
1 KV	Y			Y	2.5
1.4 KV	Y			Y	1
1.59 KV	Y			Y	2.5
1.8 KV	Y			Y	1
1.8 KV		Y		Y	2.5
1.9 KV	Y			Y	2.5
2 KV		Y		Y	2.5
2.5 kv		Y			1
2.6 KV	Y				1
2.8 KV	Y				1
2.8 KV				Y	2.5
2.9 KV	Y			Y	2.5
3.5 KV	Y			Y	2.5
3.5 KV		Y		Y	2.5
3.5 KV		Y		Y	2.5
3.7 KV	Y			Y	2.5
3.8 KV	Y				1
3.8 KV	Y			Y	2.5
3.9 KV		Y			1
4.05 KV	Y			Y	2.5
4.1 KV	Y				1
4.4 KV	Y			Y	2.5
4.5 KV	Y			Y	2.5
4.5 KV	Y			Y	1
4.7 KV	Y				1
4.8 KV					1
5.1 KV		Y			1
5.3 KV		Y			1
6 KV		Y		Y	1

Note: gnd means ground, Y means yes

extraction, and feature selection and classification using ANN. The first step is the pre-processing of the partial discharge signals where the nature of each discharge type will be investigated through time domain. After that, features of the corresponding partial discharge signals were extracted. These features include statistical components, and Fourier transforms components. To reduce the

dimensionality of the extracted features, one needs to further reduce the length of the feature vector using heuristic selection, and stepwise selection. In the end, feed forward back propagation neural network was trained and tested using the selected features and the corresponding scores were tabulated. The most appropriate feature vector is the one with highest score and minimum number of features.

3.2.1.1 Laboratory observations and time domain analysis

In this section, the nature of different classes of PD was investigated using the data and the observation captured in the lab. Four classes of PD experienced by composite insulators were studied.

3.2.1.1.1 Surface discharge (Class 1)

Water droplets were placed on the surface of the insulator to stimulate surface discharge. Different trials were made in different locations and arrangements. It was noticed that PD inception voltage is not a constant value. Also, it was observed that the surface discharge is not a continuous phenomena and it depends on many factors. One factor is the size of the water droplet. As the size increased, the PD appeared in much higher inception voltage than smaller size water droplet and the repetition of PD pulses became less. The reason behind this was the electric field experienced by the water droplet which led to shape deformation so that the inception voltage would be much higher than before. Another factor is the location of the PD. It was observed that PD caused by water droplets placed near HV side had lower inception voltage than PD caused by water droplets placed in the middle or near the grounded end of the insulator as shown in Table 3-2.

The more was the number of water droplets, the more it was likely to have PD pulses. An interesting observation was the effect of placing small water droplets in near vicinity to each other. This condition had the most likely of occurrence of PD signal and it simulates the condition of dew as shown in Table 3-2, where grouping indicates the condition of placing more than one water droplet near to each other. The reason behind grouping effect is that small water droplets are more stable and more resistive to electric field deformation effect than big ones. Also, the electric field at the tip of each adjacent water droplets is high, causing the cumulative electric field to increase.

It can be concluded from Table 3-2 that grouping of water droplets near HV side of the insulator was the most severe factor that led to initiate PD by very low inception voltage of only 400 V. In comparison, one water droplet placed near HV side would have PD inception voltage of 2.6 KV. Another conclusion is that there was no PD detection when placing PD near grounded side.

3.2.1.1.2 Corona Discharge from Energized and Dead End (Class 2 & 3)

Any partial discharge emitted from a metalic part is called corona. A sharp edge is placed on the energized HV plate. Different trials are made and corona signals are detected in each case. Corona inception voltage is approximately constant for the same experimental condition, same length between sharp edge and grounded end and same environmental condition.. As the distance becomes smaller, corona will be initiated in much lower inception voltage, but the possibility of sudden flashover will be higher.

Corona from dead end is almost the same as that from energized end. The main difference is that corona from dead end needs much higher inception voltage. The inception voltage of corona from dead end is 5.8 KV compared to corona from energized end which has an inception voltage around 4.3 KV at the same conditions. Figure 3-7 shows the time domain of both corona from energized and dead end.

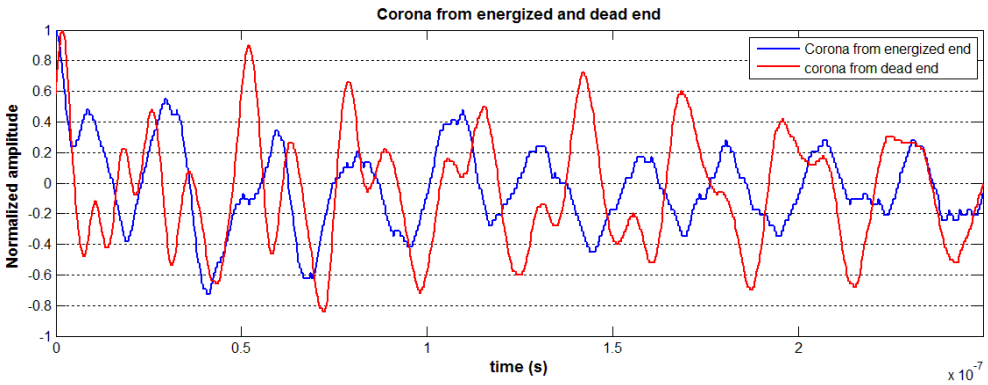

Figure 3-7: RF signal for both corona discharge from energized and dead end

3.2.1.1.3 Corona and Surface Discharge (Class 4)

A condition where there are surface discharge and corona available at the same time is studied. This condition simulates the insulator when there are problems in hardware attachment and insulator surface is polluted. Detection of both problems at

the same time will ease the corrective action process. Figure 3-8 shows the time domain of PD signal due to corona and surface discharge. To examin this case, a 2.5 cm insulator was used along with a need placed on the HV plate pointing towards a water droplet placed in the middle of the insulator. It was observed that the PD inception voltage was 3.7 KV. However, when clearing the insulator surface from any water content, it was noticed that the PD inception voltage increased to 6.4 KV which is exactly double the previous case.

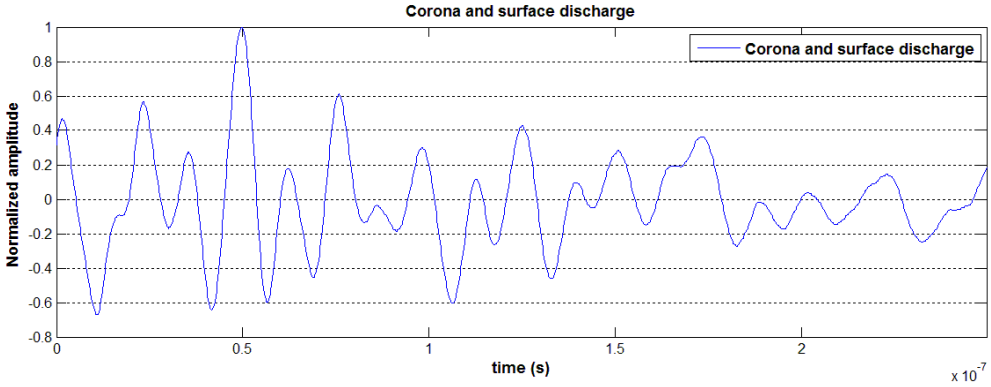

Figure 3-8: RF signal for both corona and surface discharge happening at the same time

3.2.1.2 Feature Extraction

Feature extraction is done as a preliminary stage for signal classification. Feature extraction process will be implemented using both statistical and FFT feature extraction. The total number of samples to be used is 68 samples from each class, total of 272 samples. The sampling frequency is 5 GHz and each sample would have been digitized with a total number of 2500 points.

3.2.1.2.1 Statistical Feature Extraction

To start with, time domain analysis was done for each sample. Figure 3-9 demonstrates the time domain signal for all classes.

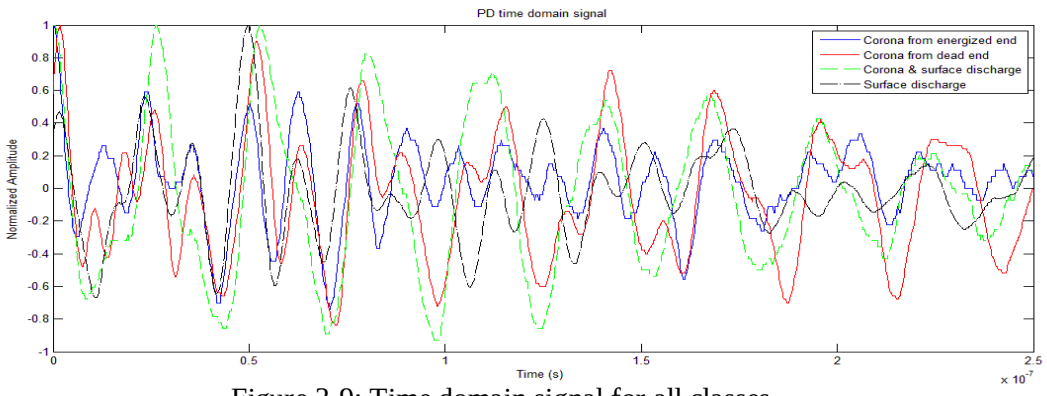

Figure 3-9: Time domain signal for all classes

As can be noticed from Figure 3-9, the time domain signals are very similar and it is very difficult to distinguish between them graphically. More investigation is done by performing statistical analysis on each signal. A comparison between each class using statistical features such as: kurtosis, skewness, mean, median, standard deviation and variance is examined. As can be noticed from Figure 3-10, Class 4 has the highest average kurtosis and the lowest average skewness while Class 3 has the lowest average kurtosis and highest average skewness. Interesting observation is that the average standard deviation between Class 1 and Class 2 is the same and between Class 3 and Class 4 is the same. However, this is only an average value and not a conclusive decision. Therefore, using the values of these statistical functions, a feature vector of size 272×6 will be formed and its validity in classification will be examined in the following sections.

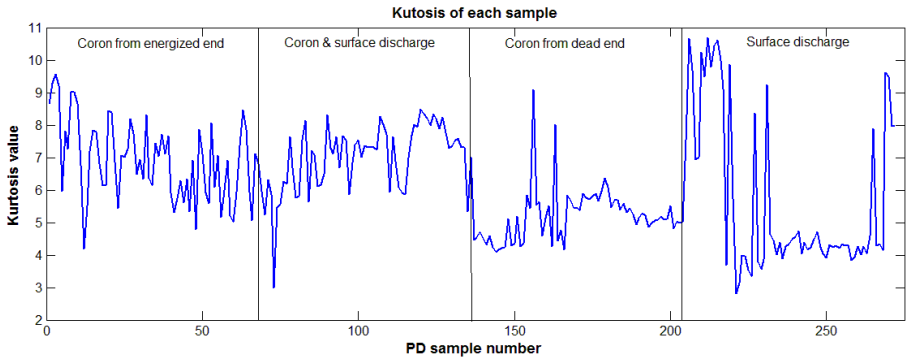

(a)

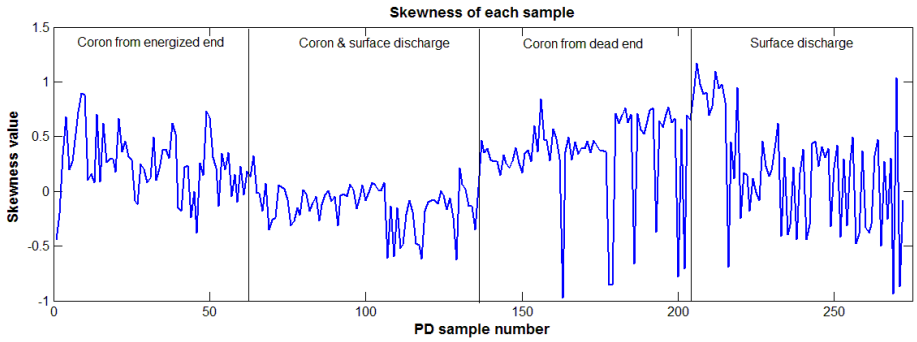

(b)

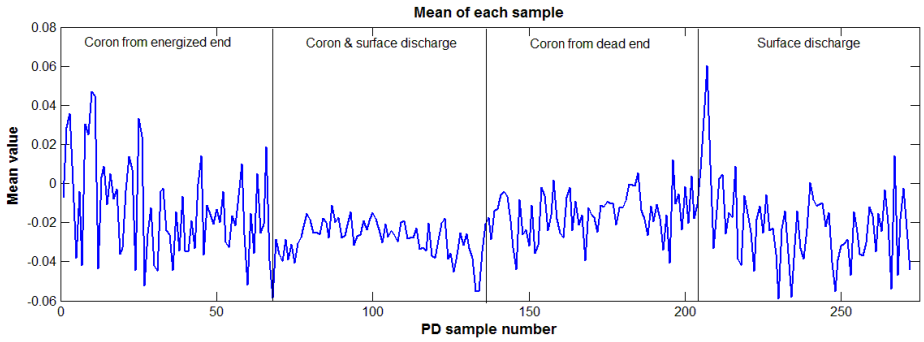

(c)

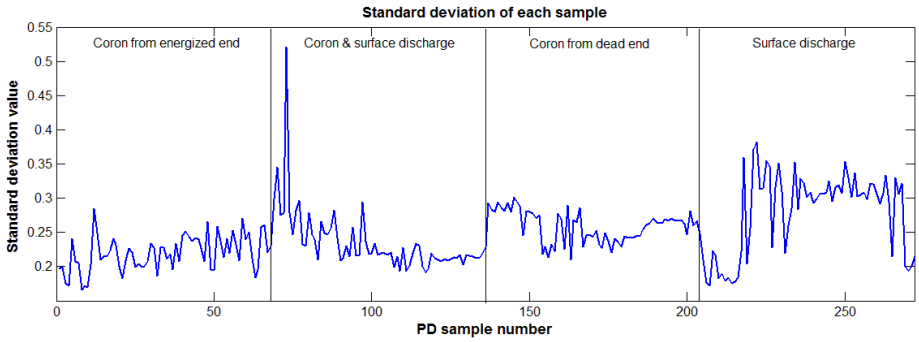

(d)

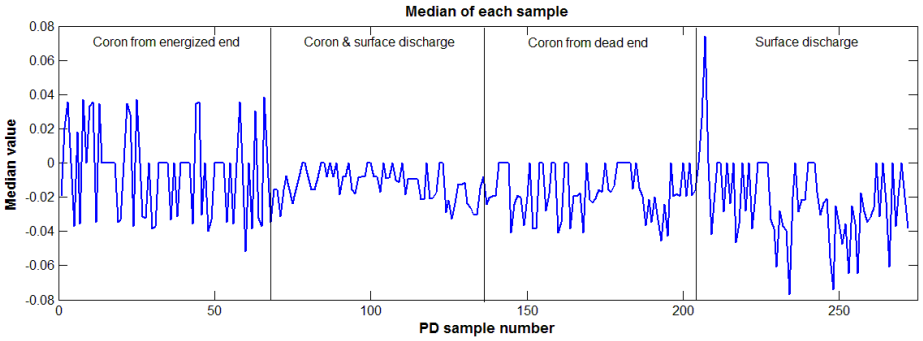

(e)

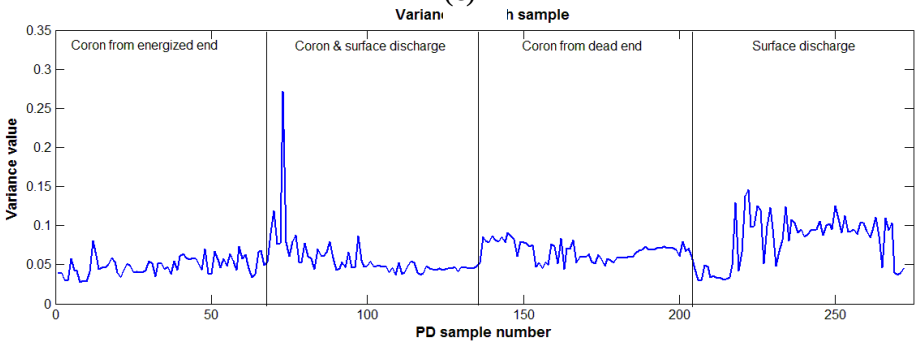

(f)

Figure 3-10: (a) Kurtosis of each sample (b) Skewness of each sample
(c) Mean of each sample (d) standard deviation of eac sample
(e) Median of each sample (f) Variance of each sample

3.2.1.2.2 Frequency Component Feature Extraction

The FFT of each PD signal is computed over 2500 points per sample. Since, the sampling frequency is 5 GHz, the corresponding frequency resolution is 2 MHz. To increase the computational frequency resolution, the time domain signal is zero padded to make its length 5000 points. Hence, the computational frequency resolution is increased to 1 MHz.

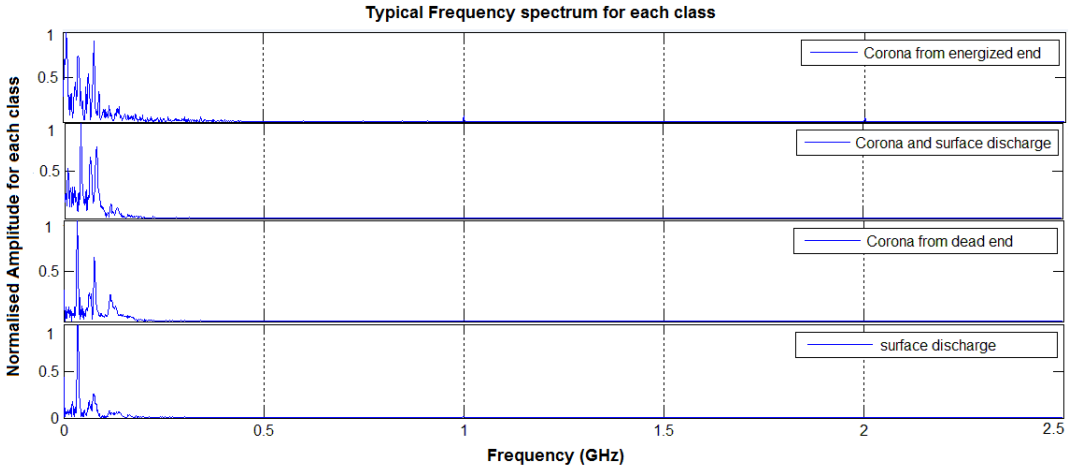

Figure 3-11: Frequency component of typical samples from each class

It is noticed from Figure 3-11 that there is no significan not information beyond 200 MHz in all PD classes. Therefore, considering an extra margin, the band of frequency was chosen to be in the range:0-499 Mhz. As a result, the FFT feature vector will be formed based on this range of frequencies with a length of 272×500.

3.2.1.3 Feature Selection and Classification using ANN

After feature extraction, the next step is to implement feature selection techniques so that the final feature vector would be ready for classification process. Feature selection methods are executed for large dimension feature vectors for two main reasons. The first reason is to reduce the dimensionality of feature vectors in order to decrease the computational time. Another reason is to select the most significant features among a given feature vector and discard the rest.

For the given feature vectors, statistical and FFT feature vectors, feature selection procedure will be implemented only to the FFT feature vector because of its large dimensionality. On the contrary, feature selection procedure will not be implemented to the statistical feature vector due to its small dimension. Rather, statistical feature vector will be directly used in ANN for classification.

In this section, the structure of back propagation neural network will be demonstrated. After that, ANN will be trained and tested using statistical fearure vector and the corresponding scores will be tabulated. Then, heurisitic and stepwise feature selection methods will be implemented against FFT feature vector, and the resulting feature vector will be used to train and test the ANN. Also, it should be noticed that the average recognition mentioned within this section is based on 15 times. At the end, a conclusion regarding the most suitable feature vector and selection method will be drown.

3.2.1.3.1 Artificial Neural Network Structure

A feed forward back propagation neural network is implemented to distinguish between the four classes:

1. Class 1: Surface Discharge.
2. Class 2: Corona from energized end.
3. Class 3: Corona from dead end.
4. Class 4: Corona + Surface discharge

The neural network structure is fixed throughout this work as demonstrated in Table 3-3

Table 3-3: Neural network structure

Structure component	Value
Number of samples used for each class	68 samples
Number of samples for testing	34
Number of samples for training	34
Number of neurons	3x(number of inputs)
Transfer function	Tansig
Training function	Traingda

3.2.1.3.2 Classification Using Statistical Feature vector:

The NN will be tested and trained using the statistical feature vector obtained from the previous section.

Table 3-4: Recognition rate of statistical feature vector

Statistical feature	Recognition Rate	Correct	Wrong
Combination of all statistical features	59.56 %	81	55

As can be noticed from Table 3-4, these statistical features don't give any significant discriminating information between the four PD classes.

3.2.1.3.3 FFT Selection and Classification Using Heuristic Method

Heuristic method is basically an iterative technique which examines the classification scores in subdivided dimension within the feature vector. Therefore, for the given FFT vector with a dimension of 500, it will be divided into 10 bands of 50 Mhz each. Then the NN will be trained and tested using the features within each band. Based on the score of each band, the most significant bands will be chosen according to certain threshold for further selection. After selecting the most important bands of 50 Mhz each, these bands will be further subdivided into bands of 10 Mhz each. Then the NN will be trained and tested using each band. Based on the score of each band, the most significant bands will be chosen according to certain threshold for further selection. After selecting the most important bands of 10 Mhz each, these bands will be further reduced to bands of 3 Mhz each. Then the NN will be trained and tested using each band. Based on the score of each band, the most significant bands will be chosen according to certain threshold. Finally, the selected bands will be combined in one feature vector and will be used for final pattern classification.

First heuristic selection using bands of 50 Mhz each

The range (0-499 Mhz) is divided into 10 divisions where each one is a feature vector consisting of 50 bins, each bin corresponds to 1 Mhz. Each feature vector will be used in the neural network individually and the output performance of each feature vector will be compared.

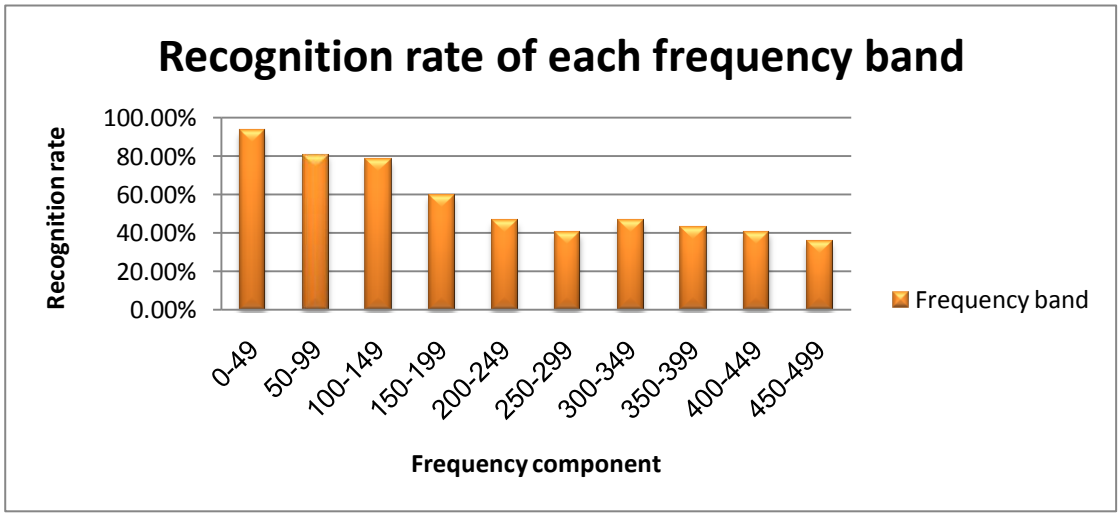

Figure 3-12: Recognition rate for bands of 50 Mhz

Figure 3-12 shows a comparison of recognition rate of each band. It is noticed that the lower range frequency contents have much better recognition rate than higher range frequency content. Considering a threshold of 80% recognition rate, the first three bands (1-99 Mhz) will be chosen for further analysis.

Second heuristic selection using bands of 10 Mhz each

In order to identify which frequency bin within each band (50 Mhz each) is more relevant, feature vector of 10 bins are examined for the selected band between 0-99 Mhz. This will result in 10 different sets of feature vectors. Figure 3-13 shows the corresponding recognition rate for these different feature vectors.

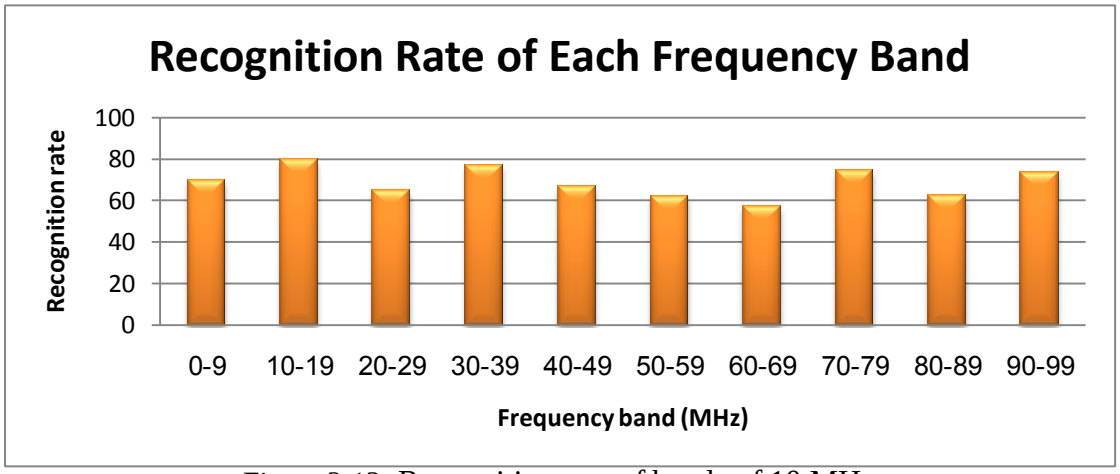

Figure 3-13: Recognition rate of bands of 10 MHz

It is noticed from Figure 3-13 that low frequency bands have more discriminating information than those higher frequency bands. Taking 70% recognition rate as threshold, five feature vectors will be considered (10-19, 30-39,70-79 and 90-99 Mhz) with a total number of 40 frequency bins.

Final heuristic selection using bands of 3 MHz each

Further reduction of dimensionality is done by considering three frequency bins per-feature vector based on the selected bands of 10 Mhz as indicated in Figure 3-14.

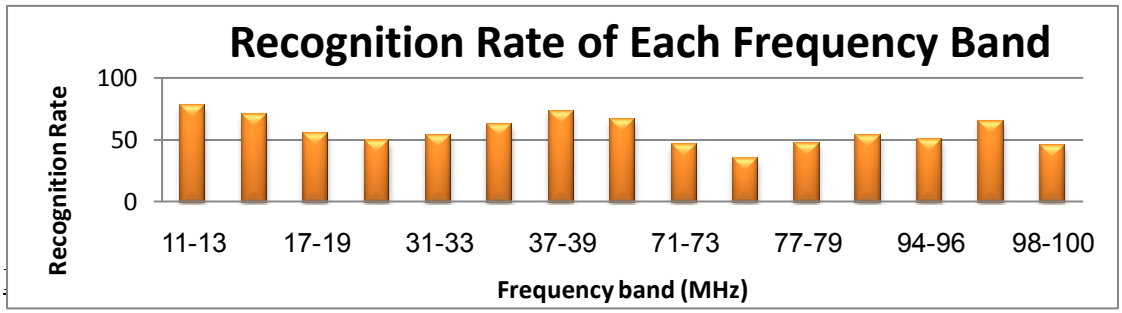

Figure 3-14: Recognition rate of bands of 3 MHz

To find better discripative feature vector, multi thresholding is performed on the resulting classification 70%, 60% and 55%. Chossing these thresholds is based on the classification results which has a maximum of 78.5%. Also, it is based on the feature vector length resulted from thresholding. The selected range of frequencies will be combined together to form more informative feature vector. As can be concluded from Table 3-5, a feature vector consisting of 22 features gives an average recognition rate of 95.2 %.

Table 3-5: The final selected FFT bands

FFT selected feature	Average recognition rate	Maximum recognition rate
70% threshold (11-16, 37-39 MHz) 9 features	88.6%	92.6%
60% threshold (11-16, 34-40, 94-96 MHz) 12 features	87.3%	94.1%
55% threshold (11-19, 34-40, 94-96, 98-100 MHz) 22 features	95.2%	97.8%

3.2.1.3.4 FFT Selection and Classification Using Stepwise Regression

Another feature selection method is the stepwise regression. This mehod is used to statistically analyze the available data and choose the most important information among them. This type of regression is very important to reduce the dimensionality of the feature vector by eliminating unnecessary information, which will result in more efficient and reliable feature vector.

A stepwise regression for the FFT feature vector (500 bins) is applied. Using all steps and default initial condition of 0.05 intering p-value threshold, the regression selected 43 features and discarded 457 features as shown in Table 3-6. It is also observed that these features are not from the same band of frequency, but spread all over the spectrum. The result shows an avergae recognition rate of 95.93 % which is good enogh for pattern classification problems. However, the length of the feature vector is still long and should be further reduced.

Table 3-6: Recognition rate of selected model using stepwise regression

Selected FFT features (MHz)	Aver –Rec-Rate	Max Rec-Rate
8,10,14,19,20,26,28,38,42,56,75,76,78,93,94,96,101,110,116,133,145,155,156,173,186,202,211,221,249,256,259,267,278,284,285,287,296,383,396,410,422,434,442	95.93 %	99.3 %

To reduce the length of the selected feature vector, the feature selection can be further fine tuned by controling the p-value for elements to be entered in the model. The default p-value is 0.05 for elements to be in the model, and 0.1 for elements to be out of the model. Using FRBM, it can be noticed that as the entering p-value threshold is decreased, the number of entering features will decrease as well.

Morever, after performing the stepwise algorithm 50 times based on different entering p-value threshold, 20 different models have been generated. The corresponding scores are shown in Table 3-7.

Table 3-7: Recognition rate of models created based on FRBM algorithm

Num of selected features	Repetition	Selected features	Average Recognition Rate
29	>=13	7,10,16,37,42,49,65,73,78,134,144,173,185,190,194,229,260,284,286,331,343,349,364,405,416,428,432,443,474	96.61765
22	>=14	7,10,37,49,65,73,78,134,144,173,185,194,229,284,286,331,364,416,428,432,443,474	95.4902
19	>=15	7,10,37,49,65,73,78,134,173,185,194,284,286,331,364,416,428,443,474	96.22549
14	>=16	7,10,37,49,65,73,78,134,173,185,194,416,428,474	95.4902
11	>=17	7,10,37,49,73,78,134,185,194,416,474	95.78431
5	>=18	7,10,73,78,416	92.35294

Note:

Models corresponding to frequency repetition rate are not mentioned because either they are of null size or they are identical to previously selected models

The classification starts with a model contains frequency features repeated most of the time. This model has the smallest length of 5 features and provides an average recognition rate of 92.4%. Then the next model contains 11 features and gives an average recognition rate of 93.1%. This process continues untill reaching the optimum recognition rate with a minimal number of features. The best classification is obtained by the last model mentioned in Table 3-7 which contains 29 features and gives an average recognition rate of 96.6%. Another feature selection method is by using VPBM algorithm. A total of 20 models are generated by altering the p-entering threshold around an initial starting value. It was found that the number of features are directly proportional with the entering p-value threshold. Therefore, the model that has the smallest length of only 4 features is the model generated using the lowest entering p-value threshold of 0.0003. When examining features within this model, it was found that the average recognition rate is about 80.5%. Then the next model to be investigated is the model generated using entering p-value threshold of 0.0034. The

total number of features within this model is 9. When exmining the features within this model, it was found that the average recognition rate is 94.55%. This process continues untill finding the model with optimum recognition rate and minimum number of features as shown in Table 3-8. It was found that the best evaluated model is the one generated using entering p-value threshold of 0.0167 with a total number of 20 features and average recognition rate of 96.37%.

Table 3-8: Recognition rate of models created based on VPBM algorithm

In-model p-value	Number of features	Selected of features	Average Rec-Rate
0.0003	4	10,101,188,416	80.49%
0.0034	9	7,10,41,73,78,101,188,416,428	94.558%
0.0098	10	7,10,41,73,78,101,188,416,428,432	91.666%
0.0122	16	7,10,37,41,49,73,78,101,134,185,188,194,416,428,432,474	94.8%
0.0156	20	7,10,37,41,49,73,78,101,134,144,173,185,188,194,272,416,428,432,472,474	94.657%
0.0167	20	7,10,37,41,49,65,73,78,101,134,144,173,185,194,272,416,428,432,472,474	96.373%
0.0191	25	7,10,37,41,49,65,73,78,101,134,144,173,185,194,272,284,286,331,364,416 ,428,432,443,472,474	95.98%
0.0227	28	7,10,37,41,49,65,73,78,101,134,144,173,185,194,229,260,272,284,286,331,364 ,405,416,428,432,443,472,474	95.54%

3.2.1.4 Summary of findings

To have a fair comparisn between each selection method used, the resulting scores and feature vector lengths are tabulated in Table 3-9. As can be concluded from Table 3-9, the smallest feature vector is obtained using VPBM with a vector size of 4 features and average recognition rate of 80.49%. Moreover, the best classification rate of 96.6% is obtained by FRBM with a feature vector length of 29 features. However, when looking to moderate feature vector length, a feature vector length of 19 features generated by FRBM is sufficient to obtain a classification of 96.22%. When comparing the classification rate of each method, it is concluded that these methods are approximately similar to each other for a given feature vector length

Table 3-9: Results comparison

Method	Aver Rec-rate	Feature vector length
VPBM	80.49%	4
FRBM	92.35294	5
VPBM	94.558%	9
VPBM	91.666%	10
FRBM	95.78431	11
FRBM	95.4902	14
VPBM	94.8%	16
FRBM	96.22549	19
VPBM	96.373%	20
FRBM	95.4902	22
Heuristic	95.2	
VPBM	95.98%	25
VPBM	95.54%	28
FRBM	96.61765	29

3.2.2 Non-Partial Discharge Identification

Partial discharge is not the only signal that might be detected using the RF sensor; rather, it can detect interference from nearby sources. One of the main interferences is the switching signal from nearby factory or crane. Switching signal appears more drastically near industrial areas and ports. The RF sensor detects both switching and PD signals, so it is necessary to differentiate between each signal. Total number of 135 switching signals were captured and compared with PD signals.

As the previous section, the same neural network structure and feature extraction process will be used in this section. However, the feature selection method that will be used is only the optimum method obtained by the previous section, that is by using the stepwise regression starting from small length feature vector based on the least p-value threshold.

3.2.2.1 Classification Using Statistical Features

The number of statistical features is 6: variance, median, standard deviation, mean, kurtosis, and skewness. When combining these features together and train the NN, the

resulted average recognition rate is 81% as shown in Table 3-10. This shows that statistical features doesn't provide significant information that is capable of discriminating between the two clasess.

Table 3-10: Recognition rate using statistical features

Statistical Features	Aver Rec-Rate	Max Rec-Rate
6 features	81%	85%

3.2.2.2 FFT Selection and Classification Using Heuristic Method

Heuristic method is basically an iterative technique which examines the classification scores in subdivided dimension within the feature vector. Therefore, for the given FFT vector with a dimension of 500, it will be divided into 10 bands of 50 Mhz each. Then the NN will be trained and tested using the features within each band. Based on the score of each band, the most significant bands will be chosen according to certain threshold for further selection. After selecting the most important bands of 50 Mhz each, these bands will be further subdivided into bands of 10 Mhz each. Then the NN will be trained and tested using each band. Based on the score of each band, the most significant bands will be chosen according to certain threshold for further selection. After selecting the most important bands of 10 Mhz each, these bands will be further reduced to bands of 3 Mhz each. Then the NN will be trained and tested using each band. Based on the score of each band, the most significant bands will be chosen according to certain threshold. Finally, the selected bands will be combined in one feature vector and will be used for final pattern classification.

First heuristic selection using bands of 50 Mhz each

The range (0-499 Mhz) is divided into 10 divisions where each one is a feature vector consisting of 50 bins, each bin corresponds to 1 Mhz. Each feature vector will be used in the neural network individually and the output performance of each feature vector will be compared. Figure 3-15 shows a comparison of recognition rate of each band. It is noticed that the lower range frequency contents have much better recognition rate than higher range frequency content. Considering a threshold of 80% recognition rate, the first three bands (1-99 Mhz) will be chosen for further analysis.

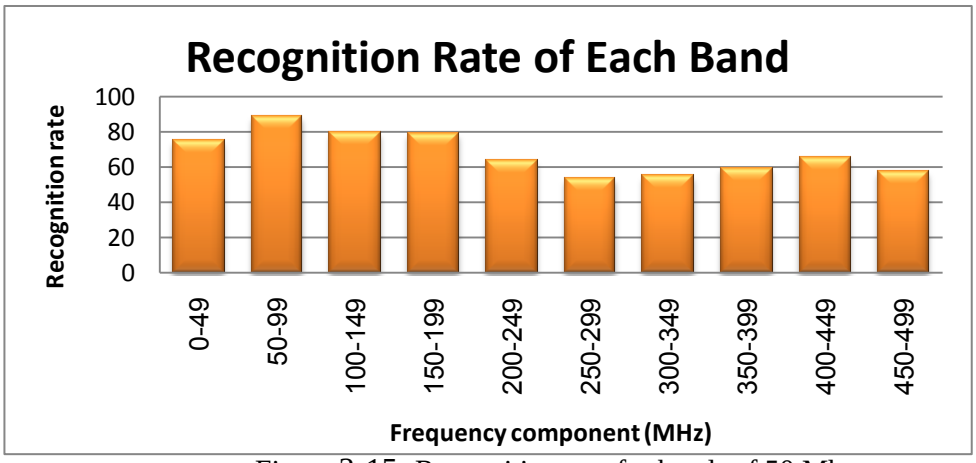

Figure 3-15: Recognition rate for bands of 50 Mhz

Second heuristic selection using bands of 10 Mhz each

In order to identify which frequency bin within each band (50 Mhz each) is more relevant, feature vector of 10 bins are examined for the selected band between 0-99 Mhz. This will result in 10 different sets of feature vectors. Figure 3-16 shows the corresponding recognition rate for these different feature vectors.

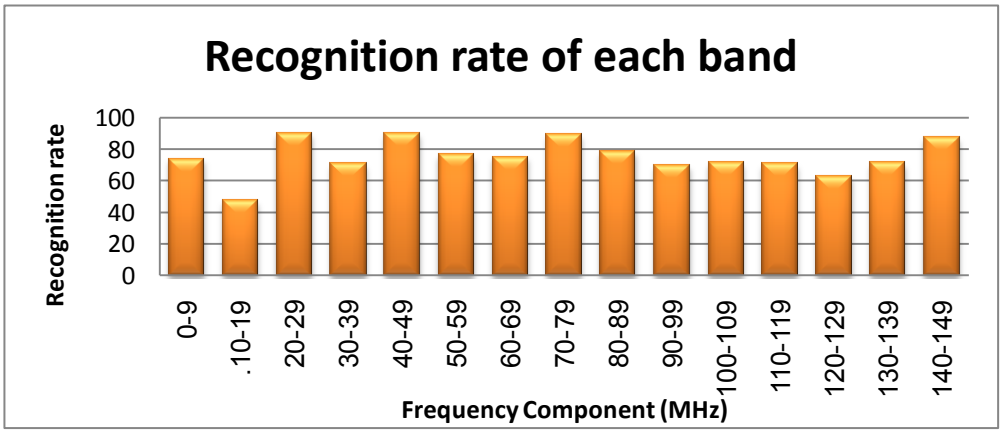

Figure 3-16: Recognition rate of bands of 10 MHz

It is noticed from Figure 3-16 that low frequency bands have more discriminating information than those higher frequency bands. Taking 85% recognition rate as threshold, five feature vectors will be considered (20-29, 40-49,70-79 and 140-169 Mhz) with a total number of 60 frequency bins.

Final heuristic selection using bands of 3 MHz each

Further reduction of dimensionality is done by considering three frequency bins per-feature vector based on the selected bands of 10 Mhz as indicated in Figure 3-17.

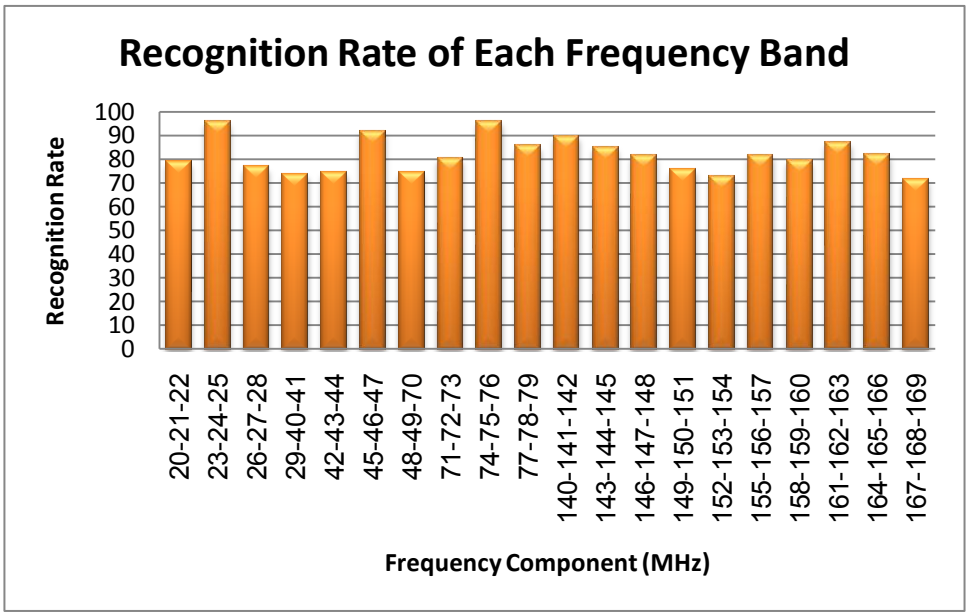

Figure 3-17: Recognition rate of bands of 3 MHz

FFT Final Selected Range

To find better discripative feature vector, multi thresholding is performed on the resulting classification 90% and 85%. Chossing these thresholds is based on the classification results which has a maximum of 96%. Also, it is based on the feature vector length resulted from thresholding. The selected range of frequencies will be combined together to form more informative feature vector. As can be concluded from Table 3-11, a feature vector consisting of 18 features gives an average recognition rate of 98.03 % which is suitable enough for classification.

Table 3-11: The final selected FFT bands

FFT selected feature	Average recognition rate	Maximum recognition rate
85% threshold (24-26, 46-48, 75-80, 141-143, 162-164 MHz) 18 features	98.03%	99.26%
90% threshold (24-26, 46-48, 75-77 MHz) 9 features	89.12%	99.26%

3.2.2.3 FFT Selection and Classification Using Stepwise Regression

A stepwise regression for the FFT feature vector (500 bins) is applied. Using all steps and default initial condition of 0.05 intering p-value threshold, the regression selected 127 features and discarded 373 features as shown in Table 3-12. It is also observed that these features are not from the same band of frequency, but spread all over the spectrum. The result shows an avergae recognition rate of 70.5 % and a maximum recognition rate of 97.5%. More investigation is made by implementing FRBM and VPBM algorithms.

Table 3-12: selected frequency range using stepwise regression

Selected FFT features (MHz)	Aver –Rec-Rate	Max Rec-Rate
3,6,7,9,13,15,18,21,23,26,28,29,31 40,47,55,57,60,76,77,79,87,89,100 104,106,109,115,116,118,119,120 125,130,131,132,138,140,141,144 145,146,148,149,158,159,161,163 165,169,172,173,178,180,187,191, 192,195,198,200,202,203,206,211, 214, 215,216,231,242,244,245,246 254,266,269,271,273,277,278,283 289,294,306,308,316,319,325,327 330,332,333,335,337,343,349,351 361,368,379,381,390,392,393,394 396,402,405,414,429,433,434,435 437,438,440,443,451,454,456,468 474,480,481,484,490,497,500	70.49%	97.5 %

To reduce the length of the selected feature vector, the feature selection can be further fine tuned by controling the p-value for elements to be entered in the model. The default p-value is 0.05 for elements to be in the model, and 0.1 for elements to be out of the model. Using FRBM, it can be noticed that as the entering p-value threshold is decreased, the number of entering features will decrease as well.

Morever, after performing the stepwise algorithm 50 times based on different entering p-value threshold, 9 different models have been generated. The corresponding scores are shown in Table 3-13.

The classification starts with a model contains frequency features repeated most of the time. This model has the smallest length of 6 features and provides an average recognition rate of 93.4%. Then the next model contains 7 features and gives an average recognition rate of 97%. This process continues untill reaching the optimum recognition rate with a minimal number of features. The best classification is obtained by the last model mentioned in Table 3-13 which contains 31 features and gives an average recognition rate of 98.08%.

Another feature selection method is by using VPBM algorithm. A total of 9 models are generated by altering the p-entering threshold around an initial starting value. It was found that the number of features are directly proportional with the entering p-value threshold. Therefore, the model that has the smallest length of only 6 features is the model generated using the lowest entering p-value threshold of 0.0012. When examining features within this model, it was found that the average recognition rate is about 93.5%. Then the next model to be investigated is the model generated using entering p-value threshold of 0.0027. The total number of features within this model is 7. When exmining the features within this model, it was found that the average recognition rate is 96.9%. This process continues untill finding the model with optimum recognition rate and minimum number of features as shown in Table 3-14. It was found that the best evaluated model is the one generated using entering p-value threshold of 0.0027 with a total number of 7 features and average recognition rate of 96.9%.

Table 3-13: Recognition rate of models created based on FRBM algorithm

Num of selected features	Repetition	Selected features	Average Recognition Rate
31	>=2	7,15,21,26,28,29,31,40,57,77,87,130,131,132,138,141,145,146,149,159,169,202,203,216,332,349,379,394,484,490,497	98.08824
15	>=3	7,15,21,26,28,57,77,87,130,132,145,169,216,332	97.2549
13	>=4	7,15,21,26,28,57,77,87,130,145,169,216,332	96.22549
11	>=5	7,15,26,28,57,77,87,130,145,16, 216	96.37255
10	>=6	7,15,26,28,57,77,87,130,145,169	97.64706
8	>=7	7,26,57,77,87,130,145,169	94.31373
7	>=8	7,26,57,77,87,130,145	97.0098
6	>9	7,26,57,77,87,145	93.38235

Note:

Models corresponding to frequency repetition rate are not mentioned because either they are of null size or they are identical to previously selected models

Table 3-14: Recognition rate of models created based on VPBM algorithm

In-model p-value	Number of features	Selected of features	Average Rec-Rate
0.0012	6	7,26,57,77,87,145	93.48039
0.0027	7	7,26,57,77,87,130,145	96.91176
0.0029	8	7,26,57,77,87,130,145,169	95.09804
0.0032	10	7,15,26,28,57,77,87,130,145,169	95.78431
0.0063	11	7,15,26,28,57,77,87,130,145,16, 216	95.14706
0.0084	13	7,15,21,26,28,57,77,87,130,145,169,216,332	96.86275
0.0284	14	7,15,21,26,28,57,77,87,130,132,145,169,216,332	93.77451
0.0448	31	7,15,21,26,28,29,31,40,57,77,87,130,131,132,138,141,145,146,149,159,169,202,203,216,332,349,379,394,484,490,497	94.60784

CHAPTER 4: CONCLUSION, APPLICATION AND FUTURE WORK

4.1 Conclusion

In summary, partial discharge online monitoring of outdoor insulator is one of the main schemes used to monitor the condition of the insulator. Such monitoring is important so as to avoid insulator failure and consequent unsustainable power loss. The current condition monitoring practices of outdoor insulators are based only on PD detection; however, detection of PD is not enough without identifying the source of PD incident so that proper corrective action could be quickly implemented. In this thesis, the main aim was to develop a comprehensive PD online monitoring system that is able to detect PD activity, identify the source of defect accurately and efficiently, and to discriminate between PD and non-PD incidents.

The main sources of defects studied are: surface discharge, corona from energized end, corona from grounded end and simultaneous corona and surface discharge. Using PD sensor, step up transformer, insulator, oscilloscope and artificial intelligence, I was able to identify specifically the defect type that causes the corresponding PD activity. Visually it was not possible to discriminate between different classes of PD wither using time or frequency domain as shown in Figure 3-9 and Figure 3-11, respectively. Therefore, artificial intelligence methods were used to discriminate between different sources of defects.

The artificial intelligence used is based on back propagation NN. The first step was to extract some important features to be used as input to the NN. The extracted features are statistical features and FFT features. After feature extraction, feature selection methods were implemented for the system to be more efficient and to operate in faster time by decreasing the number of computations. This was done using both heuristic analysis and stepwise regression techniques.

I first extracted some statistical features such as: kurtosis, skewness, median, mean, standard deviation and variance. This information was fed into the NN and scores were recorded. It was concluded that these statistical features only gave a recognition rate of 59.56% as mentioned in Table 3-4. Thus, a feature vector composed of statistical features did a poor job in discriminating between different PD sources.

The second feature vector is composed of the frequency components of time domain signal extracted using FFT algorithm. Using the Heuristic method, an average recognition rate obtained is 95.2% using a vector of 22 features. On the other hand, using stepwise regression the results were obtained using the two methods called FRBM and VPBM. Using the former method, the best obtained recognition rate was 96.6% with a feature vector of length equals to 29. It can also be noticed that a vector of 11 features gave a recognition rate of 95.7% which is comparable with the earlier obtained feature vector but with much less information. In contrast, using the later method yielded 96.4% recognition rate with a feature vector of length equals to 20.

The same procedure was implemented to discriminate between PD and non-PD signals. Using the Heuristic method, an average recognition rate obtained is 98.03% using a vector of 18 features. On the other hand, using stepwise regression the results were obtained by FRBM and VPBM. Using the former method, the best obtained recognition rate was 98.08% with a feature vector of length equals to 31. In contrast, using the later method, the best obtained recognition rate was 96.9% with a feature vector of length equals to 7.

It can be concluded that Heuristic method gives good results but it takes much more computation time than other mentioned methods and it's not systematic enough to be formulated as a generalized method. In comparison, Stepwise regression methods give more precise results than later method. When comparing between FRBM and VPBM, it is clear that they gave almost the same result for a given feature vector length. It is also concluded that more information is needed to discriminate between PD sources (~20 features) than to discriminate between PD and Non-PD (7 features).

4.2 Application and Future Work

The method introduced by this work is very important to establish a good knowledge about the condition of outdoor insulators. The main advantage of this method is its ability to not only detect PD incident, but also to identify different types of defects such as defects in energized attachment, defects in dead attachment, contamination and combination of these defects. The main application of this work is

to do effective patrol checking on outdoor insulators so that proper corrective action can be taken as illustrated in Figure 4-1.

Another application is insulator pollution estimation. This can be done by installing the PD detector permanently on certain outdoor insulators distributed in different region. When a partial discharge is detected, this means that a pollution level on these insulators installed in this region has increased and urgent cleaning would be needed to remove the source of PD signals.

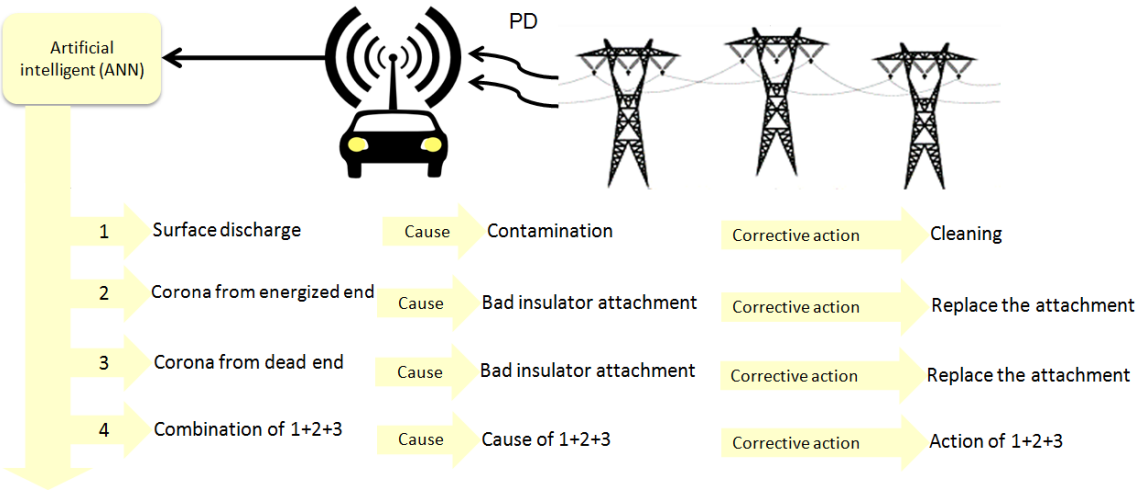

Figure 4-1: Patrol checking of outoor insulators

In future, this method can be improved using more reliable PD sensors that can detect PD signals from greater distance. Moreover, a possibility of locating PD activity would greatly aid the corrective action process. Finally, the implementation of readymade automated built in PD detection system can be investigated in terms of applicability and cost.

REFERENCES

[1] M.T. Gençoğlu, “The Comparison between Ceramic and Non-Ceramic Insulator,*” J. New World Science Academy,* pp. 274-294, Oct. 2007.

[2] R. S. Gorur et al., *Outdoor Insulators,* Ravi. S. Gorur, Inc., 1999.

[3] J. L. Goudie, M. J. Owen, T. Orbeck, "A Review of Possible Degradation Mechanisms of Silicone Elastomers in High Voltage Insulation Applications," *Conference on Electrical Insulation and Dielectric Phenomena*. vol. 1, pp. 120-127, Oct. 1998.

[4] M. Amin, M. Akbar and S. Amin, "Hydrophobicity of Silicone Rubber used for Outdoor Insulation", *Rev Adv Mater Sci.* vol. 16, no. 1-2, pp. 10-26, 2007.

[5] J. Kim et al., "Hydrophobicity Loss and Recovery of Silicone HV Insulation," *IEEE Trans. Dielectrics and Electrical Insulation,* vol. 6, no. 5, pp. 695-702, Oct. 1999.

[6] J. Kim et al., "The Mechanism of Hydrophobic Recovery of Polydimethylsiloxane Elastomers Exposed to Partial Electrical Discharge,” *J. Colloid and Interface science,* pp. 200-207, Oct. 2001.

[7] M. Amin and M. Salman, “Aging of Polymeric Insulators,” *In: Reviews on Advanced Materials Science*, vol. 13, no. 2, pp. 93-116, 2006.

[8] E. A. Cherney, "Non-Ceramic Insulators-a Simple Design that Requires Careful Analysis," *IEEE Electr. Insul. Mag.* vol. 12, no. 3, pp. 7-15, May-June, 1996.

[9] A. J. Phillips et al., "Aging of Non-Ceramic Insulators due to Corona from Water Drops," *IEEE Trans. Power Del*. vol. 14, no. 3, pp. 1081-1089, July 2009.

[10] P. J. Moore et al., "Remote Diagnosis of Overhead Line Insulation Defects," *IEEE Power Eng. Soc. General Meeting*, vol. 2, pp. 1831-1835, June 2004.

[11] S. Shihab et al., "Development of a Commercially Applicable Prototypes for On-line Monitoring of Partial Discharges and Pollution Effects on Safety of High Voltage Power Equipment," *Int. Conf. on Energy Manage. and Power Delivery, Proceedings of EMPD '98*, vol. 2, pp. 741-746, Mar. 1998.

[12] S. Chandrasekar et al. "Partial Discharge Detection as a Tool to Infer Pollution Severity of Polymeric Insulators," *IEEE Trans. Dielectr. Electr. Insul.*, vol. 17, no. 1, pp. 181-188, February 2010.

[13] V.M. Moreno and R.S. Gorur, "Accelerated Corona Discharge Performance of Polymer Compounds used in High Voltage Outdoor Insulators," *Annu. Rep. Conf. on Elect. Insulation and Dielectric Phenomena*, vol. 2, pp. 731-734, 1999.

[14] E. A. Cherney et al., "A Study of Partial Discharge from Water Droplets on a Silicone Rubber Insulating Surface," *IEEE Trans. Dielectr. Electr. Insul.*, vol. 8, no. 2, pp. 262-268, Apr. 2001.

[15] Duda et al., *Pattern Classification*, 2nd ed. New York: John Wiley and Sons, 2001.

[16] M. S. Naidu, and V. Kamaraju, *High Voltage Engineering*, 3rd ed. New York: McGraw-Hill Company Ltd, 2004.

[17] R. Hackam, "Outdoor HV Composite Polymeric Insulators," *IEEE Trans. Dielectr. Electr. Insul.*, vol. 6, no. 5, pp. 557-585, Oct. 1999.

[18] A. E. Vlastos and T. Orbeck, "Outdoor Leakage Current Monitoring of Silicone Composite Insulators in Coastal Service Conditions," *IEEE Trans. Power Del.*, vol. 11, no. 2, pp. 1066-1070, 1995.

[19] J. P. Holtzhausen and W. Vosloo, "The Leakage Current Performance Under Severe Coastal Pollution Conditions of Identically Shaped Insulators Made of Different Materials," *12th Int. Symp. on High Voltage Eng.*, Banglore, India, August, 2001.

[20] T. G. Gustavsson and S. M. Gubanski, "Leakage Current on Silicone Rubber Samples in a Coastal Environment," *12th Int. Symp. on High Voltage Eng.*, Banglore, India, August 2001.

[21] D. Windma et al., "Leakage Current Analysis and Infrared Spectroscopy of Outdoor Insulating Materials Aged in a Salt-fog Test," *IEEE Annu. Rep., Conf. on Elect. Insulation and Dielectric Phenomena*, pp. 428-432, 20-23 October, 1996.

[22] Suwarno, "Study on the Wave form of Leakage Current on the 20 kV post-pin Ceramic Insulators under various Conditions," *Int. Symp. on Elect. Insulating Materials*, pp. 387-390, 2001.

[23] M. Hikita et al., "Cross-equipment Evaluation of Partial Discharge Measurement and Diagnosis Techniques in Electric Power Apparatus for Transmission and Distribution," *IEEE Trans. Dielectr. Electr. Insul.*, vol. 15, no. 2, pp. 505-518, April 2008.

[24] M. D. Judd and I. B. B. Li Yang Hunter, "Partial Discharge Monitoring of Power Transformers using UHF Sensors. Part I: Sensors and Signal

Interpretation," *IEEE Electr. Insul. Mag.*, vol. 21, no. 2, pp. 5-14, March-April, 2005.

[25] S. Kobayashi et al., "Development of Composite Insulators for Overhead Lines (Part 2)," *Furukawa Review*, no. 21, pp. 56-61, 2002.

[26] V. M. Moreno and R. S. Gorur, "Effect of Long-term Corona on Non-ceramic Outdoor Insulator Housing Materials," *IEEE Trans. Dielectr. Electr. Insul.*, vol. 8, no. 1, pp. 117-128, Mar. 2001.

[27] S. W. Smith, *The Scientist and Engineer's Guide to Digital Signal Processing*, 2nd ed. San Diego, California Technical Publishing, 2003.

[28] P. Joaquim and S. Marques, *Applied Statistics Using SPSS, STATISTICA, MATLAB and R*, 2nd ed. Berlin, Germany, Springer, 2007.

[29] D. Howar and B. Mark, *Neural Network Toolbox For Use with MATLAB*, The MathWorks, Inc., 2000.

[30] T. Shanableh, and K. Assaleh, "Feature Modeling Using Polynomial Classifiers and Stepwise Regression," *Neurocomputing, in press Accepted Manuscript*, Mar. 2010.

VITA

Ibrahim Yehia Shurrab was born on August 23, 1985, in Abu Dhabi, UAE. He was educated in local public school and graduated from Al-Mutanabi High school. He received a scholarship by Abu Dhabi Water and Electricity Authority (ADWEA) to join the American University of Sharjah, from which he graduated in 2007. His degree was a Bachelor of Electrical Engineering.

Mr. Ibrahim moved to work in Abu Dhabi Distribution Company as a maintenance engineer in 2008. He began a master's program in Electrical Engineering at the American University of Sharjah in 2009. He was awarded the Master of Science degree in Electrical Engineering in 2011.